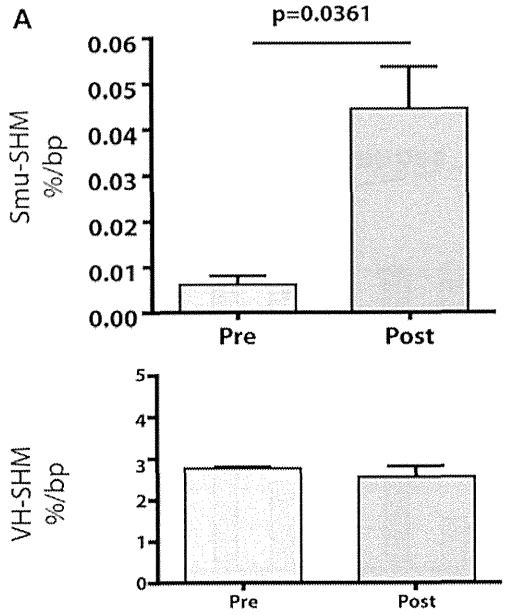

B

from \ to	A	C	G	T	sum
A		2	5	3	10
C	1		0	6	7
G	7	2		2	11
T	4	5	1		10

GC target	47.4%
GC transition	72.2%
AT transition	50.0%

FIG 2. Smu-SHMs induced by anti-CD40 mAb and IL-4 *in vitro* in PBMCs of the control subjects. **A,** Smu-SHMs were analyzed before and after stimulation of PBMCs from control subjects (n = 4) with anti-CD40 mAb and IL-4 for 5 days *in vitro*. Mutations were rarely found before stimulation (*Pre*, 0.006% ± 0.004% bp) but were significantly increased after stimulation with anti-CD40 mAb and IL-4 *in vitro* (*Post*, 0.04% ± 0.02% bp, $P = .0361$). The VH-SHMs at the JH4-JH5 region were analyzed, but no significant difference was observed because of stimulation. **B,** The Smu-SHM pattern observed after stimulation with anti-CD40 mAb and IL-4 is shown. The germline nucleotides are shown on the left *(from)*, and the mutated nucleotides are shown on the top *(to)*. The *right column* indicates the sum of the mutated nucleotides for each row. The *GC target* indicates the mutations at G or C. The *GC transition* indicates the frequency of transition mutations at G and C (G>A and C>T) of the total mutations at G and C. The *AT transition* indicates the frequency of transition mutations at A and C (A>G and T>C) of the total mutations at A and T.

and 43 RGYW motifs (172 bp, 15.2% of the length of the Smu region). In addition, 73.0% of the region is independent of either of the 2 motifs (824 bp, Fig 5).

We found 18 (unswitched memory B cells) and 41 (switched memory B cells) mutations in the WRCY motifs, which correspond to 1.12- and 1.35-fold increases in mutations compared with the expected number, respectively. Similar to the findings obtained in the analysis of the WRCY motif, we found 26 and 64 mutations in the RGYW motif, which correspond to 1.51- and 1.97-fold more mutations than expected, respectively. Thus Smu-SHMs tended to be observed within the WRCY/RGYW motifs. The C nucleotide was the preferential target in the WRCY motif because this nucleotide was the target in 52% and 51% of the mutations that were observed in unswitched memory and switched memory B cells, respectively. The G nucleotide was preferentially targeted in the RGYW motifs because it was the target in 50% and 51% of the mutations observed in unswitched memory and switched memory B cells, respectively. Outside the WRCY/RGYW motifs, the A and T nucleotides were predominantly mutated in both switched (60%) and unswitched (62%) memory B cells. The mutations at A were as frequent as those at T. In unswitched memory B cells 75.6% of the mutations at A/T were found within the WA/TW motifs, and WA/TW to WG/TC mutations accounted for 52.9% of the mutations in WA/TW motifs. In switched memory B cells 55.7% of the mutations at A/T were found within the WA/TW motifs, and WA/TW to WG/TC mutations accounted for 43.6% of the mutations in WA/TW motifs.

Smu-SHM in CD40L-, AID-, and UNG-deficient patients

To assess the CD40L, AID, and UNG dependency of the CSR process in human B cells, we analyzed the Smu-SHMs in peripheral blood purified B cells from age-matched control subjects (C1-C7) and 5 AID-deficient (P1-P5), 2 UNG-deficient (P6 and P7), and 4 CD40L-deficient (P8-P11) patients. There was no significant difference in the frequency of Smu-SHMs in $CD27^+$ memory B cells from control adults (C1-C4) and control children (C5-C7; Fig 6, *A*).

The frequencies of Smu-SHM were decreased, and small deletions were not observed (Table I) in both $CD27^+$ and $CD27^-$ B cells (Fig 6, *A*, and data not shown) in the AID- and CD40L-deficient patients, indicating the dependence of Smu-SHM on AID and CD40L. The mutation pattern of the CD40L-deficient patients was not significantly different from that of the control subjects (Fig 6, *B*). Of the 2 UNG-deficient patients,[2] P6, who has a homozygous missense mutation, presented a significantly decreased frequency of Smu-SHMs in both $CD27^+$ and $CD27^-$ B cells, and P7, who has homozygous 2-bp deletions, exhibited an increased Smu-SHM frequency in $CD27^+$ B cells but a decreased frequency in $CD27^-$ B cells (Fig 6, *A*, and data not shown). This discrepancy cannot be related to the patient's age because no difference in the Smu-SHM frequency was observed according to age (Fig 6, *A*). None of the UNG-deficient patients had small deletions in the Smu region (Table I). An important finding is that Smu-SHMs exhibited significant and characteristic bias to transitions at G and C nucleotides in both patients

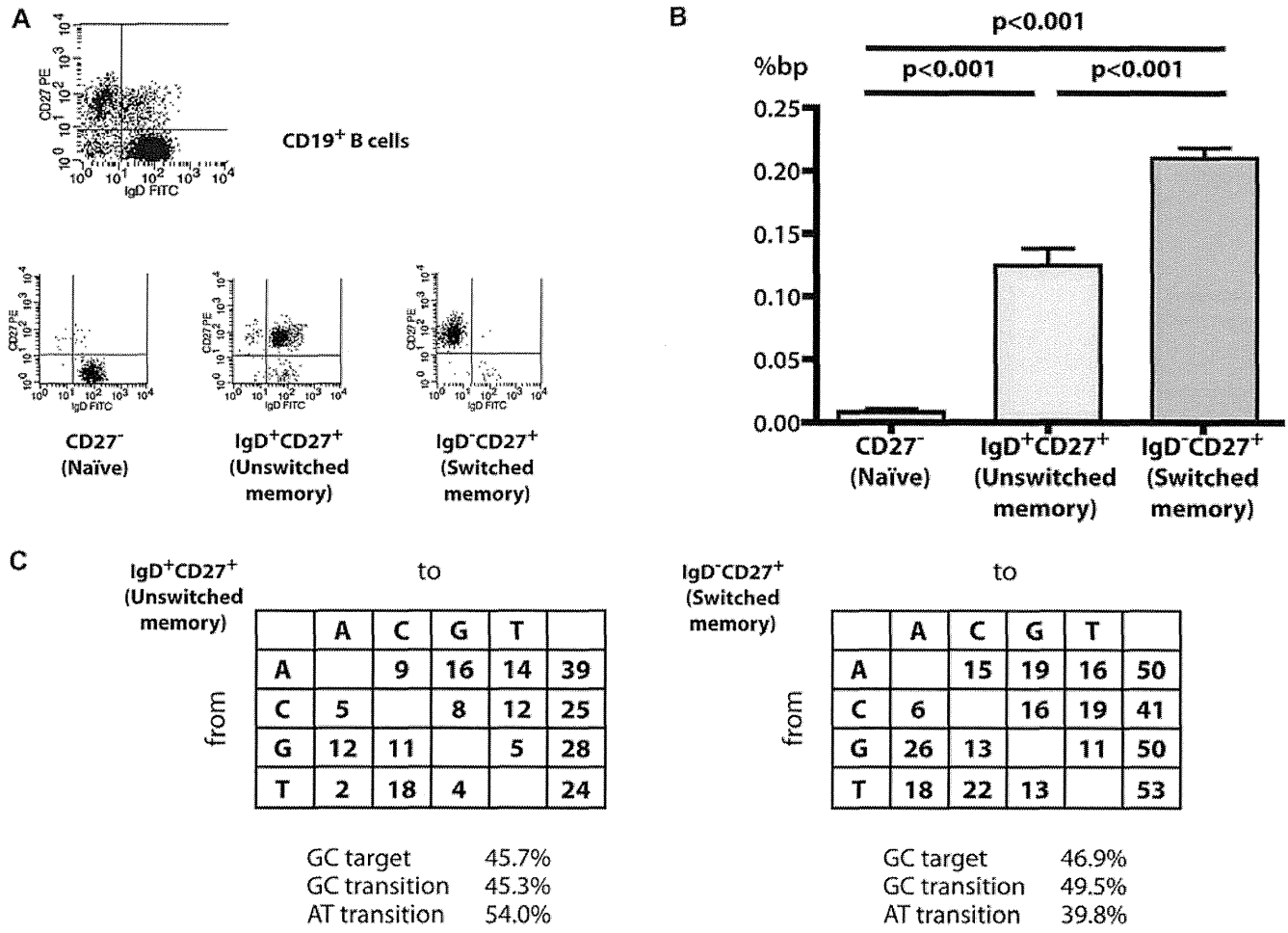

FIG 3. *In vivo* Smu-SHMs in control subjects. **A,** We purified $IgD^+IgM^+CD27^-$ (naive), $IgD^+IgM^+CD27^+$ (unswitched memory), and $IgD^-IgM^-CD27^+$ (switched memory) B cells from control subjects (n = 4) using fluorescence-activated cell sorting. Representative fluorescence-activated cell sorting data are shown. **B,** We found a higher frequency of Smu-SHMs in $IgD^-IgM^-CD27^+$ B cells, which are class-switched, and V region–mutated B cells, than in $IgD^+IgM^+CD27^+$ B cells, which are V region mutated but not class-switched B cells. The $IgD^+IgM^+CD27^-$ (naive) B cells presented the lowest frequency of Smu-SHMs. **C,** The mutation patterns of unswitched *(left)* and switched *(right)* memory B cells are shown.

(Fig 6, *B*). In contrast, A/T-targeted mutations were observed in P7, similarly to the control subjects. These results demonstrate the contribution of UNG to the formation of Smu-SHMs during CSR.

DISCUSSION

We demonstrated that SHMs occur in the Smu region in not only *in vivo* CSR-induced human B cells but also B cells activated *in vitro* with anti-CD40 mAb and IL-4, a combination that induces AID expression and CSR but not V-SHM.[14] Because the V and S regions are both transcribed on stimulation, the discrepancy between V-SHM and S-SHM occurrence *in vitro* might be related to the R-loop structure of the S (but not V) region, likely because of differences in G/C content or secondary structure.[8]

In fact, we found a significant amount of mutations in the Smu region of switched memory B cells. This amount was more than 4-fold higher than the frequency observed in B cells stimulated *in vitro*. We also found that unswitched memory B cells presented more Smu-SHMs than naive B cells, suggesting that the unswitched memory B-cell subpopulation contains a fraction that has unsuccessfully undergone CSR after the introduction of AID deamination and error-free DNA repair. These results indicate that Smu-SHMs are closely associated with CSR both *in vivo* and *in vitro* and suggest that Smu-SHMs precede the completion of CSR.

We observed significantly more mutations in the 3′ part than the 5′ part of the Smu region, even though the distribution of all of the nucleotides and the WRCY/RGYW motifs are equivalent throughout the region. Although the sequenced region is outside of the Smu core region with highly repetitive, G/C-rich sequences, this region is also known to form the R-loop with single-stranded DNA and a DNA-RNA hybrid.[16] As observed in the Smu core region, this R-loop structure might allow the accessibility of DNA to AID-induced deamination. The preferential targeting of Smu-SHMs to the 3′ part of the Smu region might reflect the frequency of the deamination of AID during CSR. Furthermore, we found more Smu-SHMs in the 5′ part of the Smu region of $IgD^-IgM^-CD27^+$ class-switched memory B cells than in the Smu region of $IgD^+IgM^+CD27^+$ unswitched memory B cells

TABLE I. *In vivo* Smu-SHMs in control subjects and patients

		$IgD^+IgM^+CD27^+$ (unswitched memory)						$IgD^-IgM^-CD27^+$ (switched memory)					
		Total clones	Mutated clones	Percentage	Clones with small deletions	Percentage	Length of small deletions (bp)	Total clones	Mutated clones	Percentage	Clones with small deletions	Percentage	Length of small deletions (bp)
C1	Adult control subjects	23	5	22	1	20	1	21	15	71	2	13	30, 72
C2		21	8	38	3	38	1, 1, 11	21	15	71	1	7	1
C3		19	7	37	1	14	8	20	10	50	1	10	5
C4		21	11	52 $CD27^+$	0	0	—	21	14	67	1	7	8, 28
C5	Age-matched control subjects	18	5	28	0	0	—						
C6		19	11	58	0	0	—						
C7		19	8	42	4	50	2, 11, 12, 25						
P1	AID deficiency	22	2	9	0	0	—						
P2		18	0	0	0	0	—						
P3		21	3	14	0	0	—						
P4		11	0	0	0	0	—						
P5		13	0	0	0	0	—						
P6	UNG deficiency	34	4	12	0	0	—						
P7		20	17	85	0	0	—						
P8	CD40L deficiency	20	10	50	0	0	—						
P9		20	3	15	0	0	—						
P10		23	1	4	0	0	—						
P11		22	4	18	0	0	—						

The genomic DNA from the purified unswitched memory and switched memory B cells of adult control subjects (C1-C4) and $CD27^+$ memory B cells from age-matched control subjects (C5-C7) and patients with AID (P1-P5), UNG (P6-P7), and CD40L (P8-P11) deficiency was analyzed for Smu-SHMs. *Total clones* indicates analyzed clones. *Mutated clones* indicates clones with at least 1 mutation. The percentage indicates the proportion of mutated clones in the total clones. The number and proportion of clones with small deletions are also shown. The length of small deletions (in base pairs) is indicated for each subject.

(Fig 3, *A*). This finding might suggest that the R-loop extension in the 5′ region of the S region contributes to CSR by opening the chromatin structure of this region to allow access for AID (see Fig E1 in this article's Online Repository at www.jacionline.org).[16] The R-loop is a characteristic structure of the S region. Our observation is consistent with the finding that the R-loop is wider in the 5′ region than formerly considered. This widespread R-loop formation might be important for CSR by opening the chromatin structure or some other unknown mechanism. These results indicate that Smu-SHMs start in the 3′ region and then spread to the 5′ upstream region during the CSR phase and that the R-loop might be larger in switched memory B cells than unswitched and naive B cells (see Fig E1). Thus the switched memory cells might have more chance of successful CSR than unswitched memory and naive B cells. Further study is needed to analyze the R-loop formation in the S region during the CSR stimulation by using the bisulfite modification assay[16] to prove this hypothesis.

We compared the nucleotide mutation pattern of Smu-SHMs with that of V-SHMs in memory B cells and found that the mutations at A were as frequent as those at T in the Smu-SHM both *in vivo* and *in vitro* (Figs 2, *C*, and 6, *B*). This finding for Smu-SHMs is different from that observed for V-SHMs because the frequency of V-SHMs at A residues is 2-fold higher than that found for T residues.[17] Smu-SHMs at A and T residues are dependent on MMR and the DNA polymerase eta.[18,19] In V-SHM the preference of A residues over T residues is explained by the preference for MMR molecules on the top strand of opened double-stranded DNA.[20] Our results might suggest that AID deamination and MMR contribute equally to both the top and bottom strands of the S region, which is different from the findings found for the V region and characteristic for Smu-SHMs. Because the number of mutations analyzed in this study is limited, further studies using next-generation sequencing would be helpful to elucidate these questions.[21]

We found that Smu-SHMs at C and G were limited within WRCY and RGYW motifs, respectively, whereas mutations at A and T were observed outside of these motifs *in vivo* (Fig 4). Because WRCY/RGYW motifs are known as target motifs of SHM in the V region and as a target sequence of RPA-binding phosphorylated AID,[22] this result indicates that AID is involved in Smu-SHMs, as well as V-SHMs, by inducing deamination on Smu-SHM in human B cells *in vivo*.

Stimulation with anti-CD40 mAb and IL-4, which induces Smu-SHM, does not induce V-SHM. This discrepancy might be due to the R-loop formation in the Smu region but not in the V region on stimulation *in vitro*. AID favors the single-strand DNA observed in the R-loop of Smu region, which is not formed in V regions by CSR stimulation.

To further investigate the roles of CD40L, AID, and UNG in Smu-SHMs in human B cells, we studied the B-cell subpopulations (naive and memory) from CD40L-deficient (n = 4), AID-deficient (n = 5), and UNG-deficient (n = 2) patients. The results show that Smu-SHMs were reduced in both CD40L- and AID-deficient patients, even in their $CD27^+$ B cells. This observation, which demonstrates the essential role for AID in Smu-SHM generation, similarly to that observed in V-SHM,[1] confirms data previously reported for successfully recombined Smu regions from unseparated peripheral blood B-cell populations of patients with heterozygous dominant negative AID mutations.[10]

The analysis of the UNG-deficient patients showed that the Smu-SHM frequency was decreased in one patient (P6) but increased in the other patient (P7). Because both patients lack expression of the UNG protein,[2,23] this discrepancy could not be explained by their different genotypes. In addition, the difference

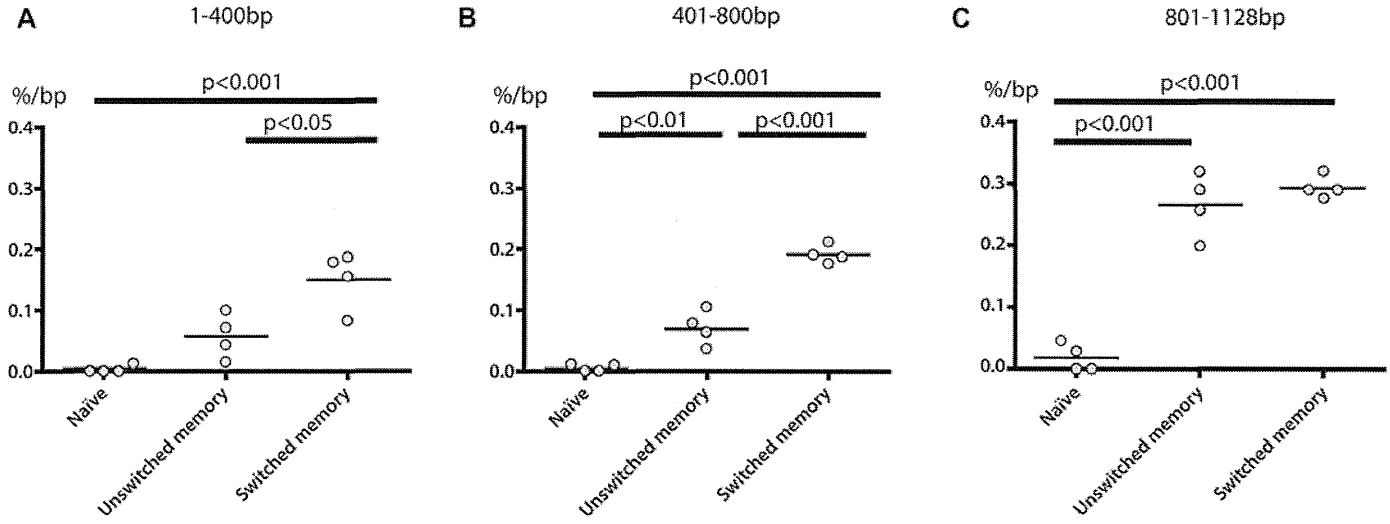

D

	Nucleotide number		
	1-400	401-800	801-1128
Naïve ($IgD^+IgM^+CD27^-$)	0.00±0.00	0.01±0.01	0.02±0.02
Unswitched memory ($IgD^+IgM^+CD27^+$)	0.06±0.04	0.07±0.03	0.27±0.05
Switched memory ($IgD^-IgM^-CD27^+$)	0.15±0.05	0.19±0.02	0.29±0.02

FIG 4. Distribution of Smu-SHMs in each fraction of control B cells *in vivo*. **A-C,** The frequency of Smu-SHMs was higher in the 3′ region than in the 5′ region in both IgD^- (switched) and IgD^+ (unswitched) fractions of $CD27^+$ B cells. **D,** Means ± SDs of Smu-SHMs in each region are shown (n = 4).

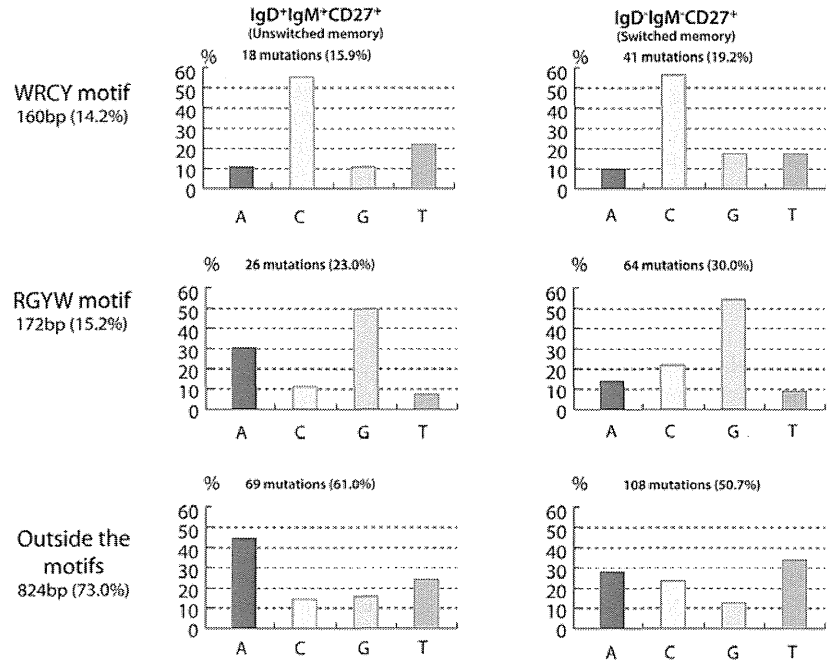

FIG 5. Target motifs of Smu-SHMs in each fraction of control B cells *in vivo*. The Smu-SHMs of the control subjects *in vivo* (n = 4) were analyzed according to their target motifs in each fraction of B cells ($IgD^+IgM^+CD27^+$ and $IgD^-IgM^-CD27^+$ B cells). *R*, Purines (A/G); *W*, A/T; *Y*, pyrimidines (C/T).

does not appear to be related to age because we did not observe any discrepancy between B cells from children and adult control subjects (Fig 6, *A*). Neither of the 2 UNG-deficient patients had small deletions in the Smu region. Smu-SHMs exhibited a skewed pattern similar to that seen in V-SHM[2] (ie, an excess of transitions on G and C nucleotides [G to A, 100%; C to T, 98.4%]) and an

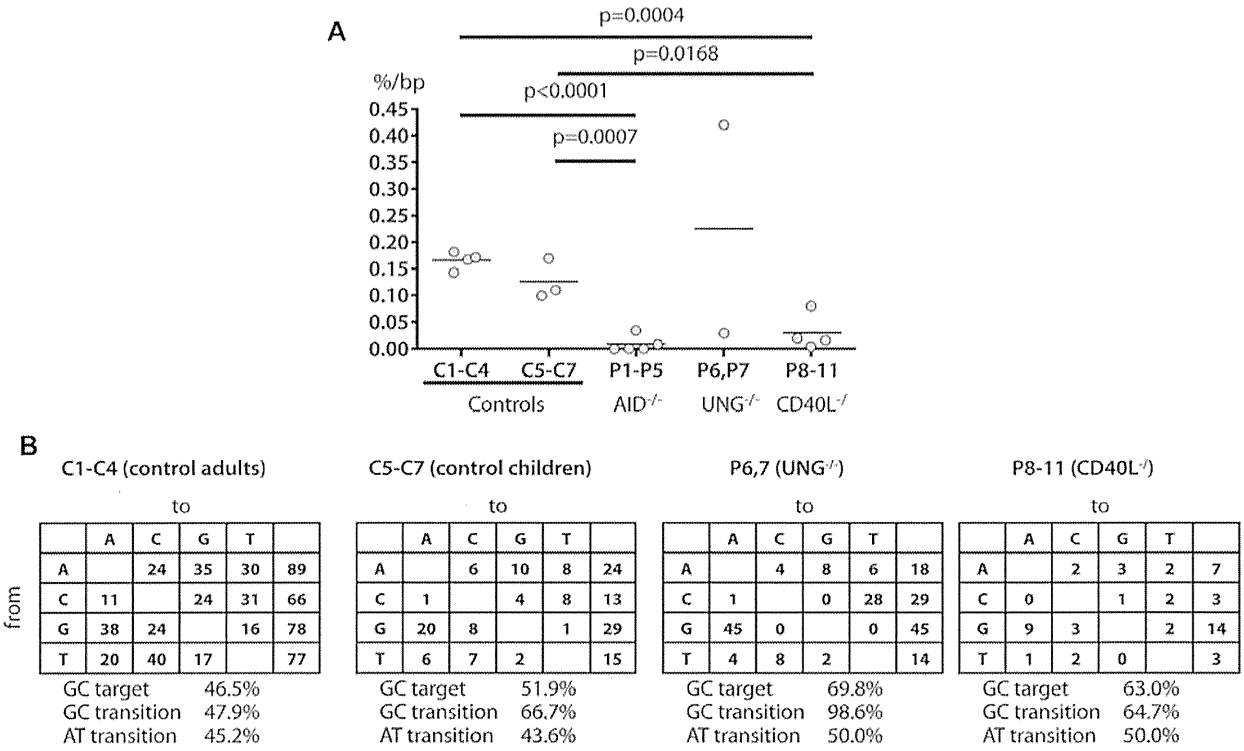

FIG 6. Smu-SHMs in patients with CD40L, AID, and UNG deficiency *in vivo*. **A,** Smu-SHMs in the $CD27^+$ fraction of B cells from control adults (C1-C4), control children (C5-C7), and AID-deficient (P1-P5), UNG-deficient (P6 and P7), and CD40L-deficient (P8-11) patients. The frequency of Smu-SHMs was decreased in patients with AID (P1-P5) and CD40L (P8-11) deficiency. In patients with UNG deficiency, the Smu-SHM frequency was decreased in P6 but increased in P7. **B,** The mutations were significantly targeted and biased to transition at G and C in UNG-deficient patients (P6 and P7).

increased targeting of G and C in both patients. This result indicates that in the absence of UNG, CSR-induced AID-dependent deaminated cytidines on both strands of the S region lead to transition mutations during their replications.

In contrast, we found normal mutation patterns at A and T in both UNG-deficient patients. The U/G mismatch introduced by AID in the S region, similarly to that observed in the V region, can be recognized by the MMR pathway. The MMR, particularly the MSH2/MSH6 complex, has been shown to be essential in the absence of UNG for both CSR and SHM in mice.[11,19] The MLH1/PMS2 complex is also reported to be important for CSR.[24] MMR deficiencies (PMS2 and MSH6 biallelic mutations) are associated with mild CSR deficiency in human subjects.[25,26] In the V regions the recruitment of the DNA polymerase eta (POLH) by the MSH2/MSH6 complex is responsible for mutations on A/T residues.[27] However, this alternative pathway, which compensates for UNG deficiency in V-SHM and Smu-SHM, is not sufficient in human subjects to induce full CSR, as shown by the marked immunoglobulin CSR deficiency and the complete lack of small deletions in Smu regions observed in both patients. In the absence of UNG, CSR-induced AID-dependent lesions in the S regions lead to mutations occurring during their repair but are inefficient for the generation of the double-strand DNA breaks necessary for CSR in human subjects.

At present, most of the hyper-IgM syndromes caused by an intrinsic B-cell defect remain molecularly undefined.[28,29] An analysis of the frequency and occurrence of CSR-induced Smu-SHMs might be a useful tool to better understand the molecular defect in these patients and disclose the CSR mechanisms.

We thank Dr Ritsuo Nishiuchi (Kochi Health Sciences Center, Kohchi, Japan) for taking care of the patients and Ms Makiko Tanaka (National Defense Medical College, Saitama, Japan) and Ms Monique Forveille (U768, INSERM, Paris, France) for their skillful technical assistance. We also thank the critical reading performed by Dr Patrick Revy (U768, INSERM, Paris, France).

Key messages

- **CSR-induced mutations occurring in Smu-SHM were observed in both *in vitro* and *in vivo* switched and unswitched human memory B cells.**
- **The extension of SHM to the 5′ upstream region of Smu might be associated with the effective induction of CSR.**
- **Smu-SHM depends on CD40L, AID, UNG, and the MMR system.**

REFERENCES

1. Revy P, Muto T, Levy Y, Geissmann F, Plebani A, Sanal O, et al. Activation-induced cytidine deaminase (AID) deficiency causes the autosomal recessive form of the hyper-IgM syndrome (HIGM2). Cell 2000;102:565-75.
2. Imai K, Slupphaug G, Lee W-I, Revy P, Nonoyama S, Catalan N, et al. Human uracil-DNA glycosylase deficiency associated with profoundly impaired immunoglobulin class-switch recombination. Nat Immunol 2003;4:1023-8.
3. Durandy A, Revy P, Imai K, Fischer A. Hyper-immunoglobulin M syndromes caused by intrinsic B-lymphocyte defects. Immunol Rev 2005;203:67-79.
4. Yan CT, Boboila C, Souza EK, Franco S, Hickernell TR, Murphy M, et al. IgH class switching and translocations use a robust non-classical end-joining pathway. Nature 2007;449:478-82.

5. Chaudhuri J, Alt FW. Class-switch recombination: interplay of transcription, DNA deamination and DNA repair. Nat Rev Immunol 2004;4:541-52.
6. Nagaoka H, Muramatsu M, Yamamura N, Kinoshita K, Honjo T. Activation-induced deaminase (AID)-directed hypermutation in the immunoglobulin Smu region: implication of AID involvement in a common step of class switch recombination and somatic hypermutation. J Exp Med 2002;195:529-34.
7. Schrader CE, Vardo J, Stavnezer J. Mlh1 can function in antibody class switch recombination independently of Msh2. J Exp Med 2003;197:1377-83.
8. Peled JU, Kuang FL, Iglesias-Ussel MD, Roa S, Kalis SL, Goodman MF, et al. The biochemistry of somatic hypermutation. Annu Rev Immunol 2008;26: 481-511.
9. Muramatsu M, Kinoshita K, Fagarasan S, Yamada S, Shinkai Y, Honjo T. Class switch recombination and hypermutation require activation-induced cytidine deaminase (AID), a potential RNA editing enzyme. Cell 2000;102: 553-63.
10. Kracker S, Imai K, Gardës P, Ochs HD, Fischer A, Durandy AH. Impaired induction of DNA lesions during immunoglobulin class-switch recombination in humans influences end-joining repair. Proc Natl Acad Sci U S A 2010;107:22225-30.
11. Xue K, Rada C, Neuberger MS. The in vivo pattern of AID targeting to immunoglobulin switch regions deduced from mutation spectra in msh2-/- ung-/- mice. J Exp Med 2006;203:2085-94.
12. Zhu Y, Nonoyama S, Morio T, Muramatsu M, Honjo T, Mizutani S. Type two hyper-IgM syndrome caused by mutation in activation-induced cytidine deaminase. J Med Dent Sci 2003;50:41-6.
13. Fecteau JF, Néron S. CD40 stimulation of human peripheral B lymphocytes: distinct response from naive and memory cells. J Immunol 2003;171:4621-9.
14. Nonoyama S, Hollenbaugh D, Aruffo A, Ledbetter JA, Ochs HD. B cell activation via CD40 is required for specific antibody production by antigen-stimulated human B cells. J Exp Med 1993;178:1097-102.
15. Warnatz K, Denz A, Dräger R, Braun M, Groth C, Wolff-Vorbeck G, et al. Severe deficiency of switched memory B cells (CD27(+)IgM(-)IgD(-)) in subgroups of patients with common variable immunodeficiency: a new approach to classify a heterogeneous disease. Blood 2002;99:1544-51.
16. Huang F-T, Yu K, Balter BB, Selsing E, Oruc Z, Khamlichi AA, et al. Sequence dependence of chromosomal R-loops at the immunoglobulin heavy-chain Smu class switch region. Mol Cell Biol 2007;27:5921-32.
17. Neuberger MS, Noia JMD, Beale RCL, Williams GT, Yang Z, Rada C. Somatic hypermutation at A·T pairs: polymerase error versus dUTP incorporation. Nat Rev Immunol 2005;5:171-8.
18. Faili A. DNA polymerase is involved in hypermutation occurring during immunoglobulin class switch recombination. J Exp Med 2004;199:265-70.
19. Rada C, Di Noia JM, Neuberger MS. Mismatch recognition and uracil excision provide complementary paths to both Ig switching and the A/T-focused phase of somatic mutation. Mol Cell 2004;16:163-71.
20. Unniraman S, Schatz DG. Strand-biased spreading of mutations during somatic hypermutation. Science 2007;317:1227-30.
21. Perez-Duran P, Belver L, de Yebenes VG, Delgado P, Pisano DG, Ramiro AR. UNG shapes the specificity of AID-induced somatic hypermutation. J Exp Med 2012;209:1379-89.
22. Chaudhuri J, Khuong C, Alt FW. Replication protein A interacts with AID to promote deamination of somatic hypermutation targets. Nature 2004;430:992-8.
23. Kavli B, Andersen S, Otterlei M, Liabakk NB, Imai K, Fischer A, et al. B cells from hyper-IgM patients carrying UNG mutations lack ability to remove uracil from ssDNA and have elevated genomic uracil. J Exp Med 2005;201:2011-21.
24. Chahwan R, van Oers JMM, Avdievich E, Zhao C, Edelmann W, Scharff MD, et al. The ATPase activity of MLH1 is required to orchestrate DNA double-strand breaks and end processing during class switch recombination. J Exp Med 2012;209:671-8.
25. Péron S, Metin A, Gardës P, Alyanakian M-A, Sheridan E, Kratz CP, et al. Human PMS2 deficiency is associated with impaired immunoglobulin class switch recombination. J Exp Med 2008;205:2465-72.
26. Gardës P, Forveille M, Alyanakian M-A, Aucouturier P, Ilencikova D, Leroux D, et al. Human MSH6 deficiency is associated with impaired antibody maturation. J Immunol 2012;188:2023-9.
27. Delbos F, Aoufouchi S, Faili A, Weill J-C, Reynaud C-A. DNA polymerase eta is the sole contributor of A/T modifications during immunoglobulin gene hypermutation in the mouse. J Exp Med 2007;204:17-23.
28. Imai K, Catalan N, Plebani A, Marodi L, Sanal O, Kumaki S, et al. Hyper-IgM syndrome type 4 with a B lymphocyte-intrinsic selective deficiency in Ig class-switch recombination. J Clin Invest 2003;112:136-42.
29. Péron S, Pan-Hammarström Q, Imai K, Du L, Taubenheim N, Sanal O, et al. A primary immunodeficiency characterized by defective immunoglobulin class switch recombination and impaired DNA repair. J Exp Med 2007;204:1207-16.

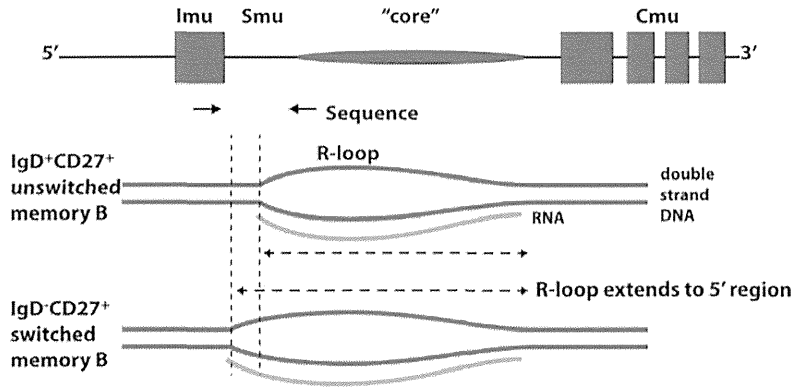

FIG E1. Smu-SHMs might correspond to the extension of the R-loop. We found more mutations in the 3′ part of the sequenced region, which is close to the Smu core region, than in the 5′ region in both unswitched and switched memory B cells. Furthermore, we found more mutations in the 5′ part of the sequenced region in switched memory B cells than in unswitched memory B cells. These findings might indicate the extension of the R-loop during CSR.

BCG vaccination in patients with severe combined immunodeficiency: Complications, risks, and vaccination policies

Beatriz E. Marciano, MD,[a] Chiung-Yu Huang, PhD,[b] Gyan Joshi, PhD,[b] Nima Rezaei, MD,[c] Beatriz Costa Carvalho, MD,[d] Zoe Allwood, MD,[e] Aydan Ikinciogullari, MD,[f] Shereen M. Reda, MD,[g] Andrew Gennery, MD,[h] Vojtech Thon, MD,[i] Francisco Espinosa-Rosales, MD,[j] Waleed Al-Herz, MD,[k] Oscar Porras, MD,[l] Anna Shcherbina, MD,[m] Anna Szaflarska, MD,[n] Şebnem Kiliç, MD,[o] Jose L. Franco, MD, PhD,[p] Andrea C. Gómez Raccio, MD,[q] Persio Roxo, Jr, MD,[r] Isabel Esteves, MD,[s] Nermeen Galal, MD,[t] Anete Sevciovic Grumach, MD, PhD,[u] Salem Al-Tamemi, MD,[v] Alisan Yildiran, MD,[w] Julio C. Orellana, MD,[x] Masafumi Yamada, MD,[y] Tomohiro Morio, MD,[z] Diana Liberatore, MD,[aa] Yoshitoshi Ohtsuka, MD,[bb] Yu-Lung Lau, MD,[cc] Ryuta Nishikomori, MD,[dd] Carlos Torres-Lozano, MD,[ee] Juliana T. L. Mazzucchelli, MD,[d] Maria M. S. Vilela, MD,[d] Fabiola S. Tavares, MD,[d] Luciana Cunha, MD,[ff] Jorge A. Pinto, MD,[ff] Sara E. Espinosa-Padilla, MD,[j] Leticia Hernandez-Nieto, MD,[j] Reem A. Elfeky, MD,[g] Tadashi Ariga, MD,[y] Heike Toshio, MD,[dd] Figen Dogu, MD,[f] Funda Cipe, MD,[f] Renata Formankova, MD,[gg] M. Enriqueta Nuñez-Nuñez, MD,[ee] Liliana Bezrodnik, MD,[q] Jose Gonçalo Marques, MD,[s] María I. Pereira, PhD,[x] Viviana Listello, MD,[x] Mary A. Slatter, MD,[h] Zohreh Nademi, MD,[h] Danuta Kowalczyk, MD,[n] Thomas A. Fleisher, MD,[hh] Graham Davies, MD,[e] Bénédicte Neven, MD,[ii] and Sergio D. Rosenzweig, MD, PhD[jj]

Bethesda, Md, Tehran, Iran, São Paulo and Minas Gerais, Brazil, London and Newcastle upon Tyne, United Kingdom, Ankara, Bursa, and Atakum-Samsun, Turkey, Cairo, Egypt, Brno and Prague, Czech Republic, Mexico City and Guadalajara, Mexico, Kuwait City, Kuwait, San Jose, Costa Rica, Moscow, Russia, Krakow, Poland, Medellin, Colombia, Buenos Aires and Córdoba, Argentina, Lisbon, Portugal, Muscat, Oman, Sapporo, Tokyo, Hyogo, and Kyoto, Japan, Hong Kong, China, and Paris, France

Background: Severe combined immunodeficiency (SCID) is a syndrome characterized by profound T-cell deficiency. BCG vaccine is contraindicated in patients with SCID. Because most countries encourage BCG vaccination at birth, a high percentage of patients with SCID are vaccinated before their immune defect is detected.

From [a]the Laboratory of Clinical Infectious Diseases, National Institute of Allergy and Infectious Diseases, National Institutes of Health, Bethesda; [b]the Biostatistics Research Branch, National Institute of Allergy and Infectious Diseases, National Institutes of Health, Bethesda; [c]the Pediatric Center of Excellence, Children's Medical Center Hospital, Tehran University of Medical Sciences; [d]the Department of Pediatrics, Federal University of São Paulo; [e]the Immunology Department, Great Ormond Street Hospital for Children, London; [f]the Department of Pediatric Immunology and Allergy, Ankara University Medical School; [g]the Department of Pediatric Allergy and Immunology, Children's Hospital, Ain Shams University, Cairo; [h]the Paediatric Immunology Department, Great North Children's Hospital, Newcastle upon Tyne; [i]the Department of Clinical Immunology and Allergy, Medical Faculty of Masaryk University, St Anne's University Hospital, Brno; [j]the National Institute of Pediatrics, Mexico City Federal District; [k]the Department of Pediatrics, Faculty of Medicine, Kuwait University, Al-Sabah Hospital, Kuwait City; [l]the Department of Immunology and Rheumatology, National Children's Hospital "Dr. Carlos Sáenz Herrera," San Jose; [m]the Department of Clinical Immunology, Center for Pediatric Hematology, Oncology and Immunology, Moscow; [n]the Department of Clinical Immunology and Transplantology, Children's University Hospital, Krakow; [o]the Pediatric Immunology Division, Uludag University Medical Faculty, Bursa; [p]the Primary Immunodeficiency Group, University of Antioquia, Medellin; [q]the Immunology Unit, Children's Hospital Ricardo Gutierrez, Buenos Aires; [r]the Faculty of Medicine of Ribeirão Preto, University of São Paulo; [s]the Primary Immunodeficiency Center, Lisbon Academic Center, Santa María Hospital, Lisbon; [t]Cairo University; [u]Faculty of Medicine of ABC, Santo André, São Paulo; [v]the Department of Child Health, Sultan Qaboos University Hospital, Muscat; [w]the Department of Pediatric Immunology-Allergy, Ondokuz Mayis University, Atakum-Samsun; [x]the Division of Allergy and Clinical Immunology, Santísima Trinidad Children's Hospital, Córdoba; [y]the Department of Pediatrics, Hokkaido University Graduate School of Medicine, Sapporo; [z]Tokyo Medical and Dental University; [aa]Pediatric Immunology, Italian Hospital, Buenos Aires; [bb]Hyogo College of Medicine; [cc]the Department of Pediatrics and Adolescent Medicine, LKS Faculty of Medicine, University of Hong Kong; [dd]the Department of Pediatrics, Kyoto University Hospital; [ee]the Department of Clinical Immunology and Allergology, Western National Medical Center, Guadalajara; [ff]the Federal University of Minas Gerais; [gg]Charles University, and University Hospital Motol, Prague; [hh]the Immunology Service, DLM, CC, National Institutes of Health, Bethesda; [ii]the Immunology-Hematology and Rheumatology Service, Necker Hospital, Paris; and [jj]the Primary Immunodeficiency Clinic and Infectious Diseases Susceptibility Unit, LHD, National Institute of Allergy and Infectious Diseases, National Institutes of Health, Bethesda.

Supported by the Intramural Research Program of the National Institutes of Health, National Institute of Allergy and Infectious Disease. V.T. was supported by the European Community's Seventh Framework Program FP7/2007-2013 under grant agreement no. 201549 (EURO-PADnet HEALTH-F2-2008-201549).

Disclosure of potential conflict of interest: N. Rezaei is employed by and has received research support from Tehran University Med Sci, has received royalties from Springer, and has been supported by an American Academy of Allergy, Asthma & Immunology (AAAAI) Young Investigator Award. B. Costa Carvalho has received payment for development of educational presentations from the Federal University of Sao Paulo (FAPESP) and has received travel support from Octapharma. V. Thon has received research support from EURO-PADnet HEALTH (F2-2008-201549). J. L. Franco has received consultancy fees from Baxter and Kedrion and has received lecture fees from Grifols. A. Sevciovic Grumach is a board member for Latin American Society for Immunodeficiencies and has received consultancy fees and lecture fees from SHIRE and CSL. T. Morio has received grant-in-aids for scientific research from the Japan Science and Technology Agency; the Ministry of Education, Culture, and Sport; and the Ministry of Health, Labour, and Welfare in Japan and has received lecture fees from Abbvie, CSL Behring, Chugai Pharmaceutical, Meiji Pharmaceuticals, Teijin Pharma, and Toray Medical. S. D. Rosenzweig has received consultancy fees from InPractice and UpToDate. The rest of the authors declare that they have no relevant conflicts of interest.

Received for publication July 5, 2013; revised February 12, 2014; accepted for publication February 17, 2014.

Corresponding author: Sergio D. Rosenzweig, MD, PhD, Immunology Service, DLM, CC, NIH, 10 Center Dr, Bldg 10, 2C410F, Bethesda, MD 20892. E-mail: srosenzweig@cc.nih.gov.

0091-6749

http://dx.doi.org/10.1016/j.jaci.2014.02.028

Objectives: We sought to describe the complications and risks associated with BCG vaccination in patients with SCID.
Methods: An extensive standardized questionnaire evaluating complications, therapeutics, and outcomes regarding BCG vaccination in patients given a diagnosis of SCID was widely distributed. Summary statistics and association analysis was performed.
Results: Data on 349 BCG-vaccinated patients with SCID from 28 centers in 17 countries were analyzed. Fifty-one percent of the patients had BCG-associated complications, 34% disseminated and 17% localized (a 33,000- and 400-fold increase, respectively, over the general population). Patients receiving early vaccination (≤1 month) showed an increased prevalence of complications ($P = .006$) and death caused by BCG-associated complications ($P < .0001$). The odds of experiencing complications among patients with T-cell numbers of 250/μL or less at diagnosis was 2.1 times higher (95% CI, 1.4-3.4 times higher; $P = .001$) than among those with T-cell numbers of greater than 250/μL. BCG-associated complications were reported in 2 of 78 patients who received antimycobacterial therapy while asymptomatic, and no deaths caused by BCG-associated complications occurred in this group. In contrast, 46 BCG-associated deaths were reported among 160 patients treated with antimycobacterial therapy for a symptomatic BCG infection ($P < .0001$).
Conclusions: BCG vaccine has a very high rate of complications in patients with SCID, which increase morbidity and mortality rates. Until safer and more efficient antituberculosis vaccines become available, delay in BCG vaccination should be considered to protect highly vulnerable populations from preventable complications. (J Allergy Clin Immunol 2014;133:1134-41.)

Key words: *Primary immunodeficiency, severe combined immunodeficiency, vaccine, BCG, mycobacteria, newborn screening, hematopoietic stem cell transplant, immune reconstitution syndrome*

Tuberculosis is a major global health problem. In 1993, the World Health Organization (WHO) declared the disease a global public health emergency, and in 2011, one third of the world's population was thought to be infected with *Mycobacterium tuberculosis*, with almost 9 million new cases diagnosed and 1.4 million deaths attributed to this organism. In recent years, most technologically advanced countries have managed to control, although not eradicate, tuberculosis. With more than 4 billion doses applied, the live attenuated *Mycobacterium bovis* BCG vaccine has been a part of efforts to control tuberculosis and remains one of the most widely used of all current vaccines worldwide. Since the 1960s, it has been administered routinely in the majority of countries, and currently, approximately 120 million persons, mostly newborns, are vaccinated every year through national childhood immunization programs. The BCG vaccine has a documented protective effect against meningitis and disseminated tuberculosis in children; however, it does not prevent primary infection and, more importantly, does not prevent reactivation of latent pulmonary infection, the principal source of bacillary spread in the community. The effect of BCG vaccination on transmission of *M tuberculosis* is therefore limited (reviewed in Plotkin et al[1] and the Global Tuberculosis Report, 2012, WHO, http://www.who.int/tb/publications/global_report/gtbr12_main.pdf).

Abbreviations used
HSCT: Hematopoietic stem cell transplantation
IL2RG: IL-2 receptor γ
IRS: Immune reconstitution syndrome
MAT: Multidrug antimycobacterial therapy
RAG: Recombination-activating gene
SCID: Severe combined immunodeficiency
WHO: World Health Organization

Despite its long history and extensive use, there appears to be no other vaccine as controversial as BCG, and its history contains aspects of folklore and superstition that often supersede facts in public health discussions and policy.[1-3]

Severe combined immunodeficiency (SCID) includes a heterogeneous group of genetic conditions characterized by profound deficiencies in T-cell (and in some types B-cell, natural killer cell, or both) numbers and function. If untreated, infants with typical SCID succumb early in life from severe and recurrent infections. Mutations in different genes affecting cytokine signaling (eg, IL-2 receptor γ *[IL2RG]* and *IL7RA*), antigen receptor processing (eg, recombination-activating gene 1 *[RAG1]*, *RAG2*, and *CD3D*), or nucleotide processing (eg, adenosine deaminase *[ADA]*) cause this fatal childhood condition, unless immune reconstitution can be accomplished.[4] However, it should be noted that patients with severe manifestations of other syndromic conditions might have clinical signs and symptoms consistent with SCID.[5] BCG, as other live attenuated vaccines, is absolutely contraindicated in patients with SCID (as reviewed by Plotkin et al[1] and the Centers for Disease Control and Prevention[6] and the Global Tuberculosis Report, 2012, World Health Organization, http://www.who.int/tb/publications/global_report/gtbr12_main.pdf). However, because it is usually administered at birth, patients with SCID in most countries using BCG are vaccinated before their immune deficiency is diagnosed.

The aim of this study was to describe the complications and risks associated with BCG vaccination in patients given a diagnosis of SCID, the most severe form of primary immunodeficiency diseases.

METHODS

An extensive standardized questionnaire evaluating diagnostics, therapeutics, and outcomes concerning BCG-vaccinated patients with SCID was developed by an *ad hoc* scientific interest group (the "BCG infection in SCID patients interest group"; N.R., G.D., B.N., and S.D.R.; see Table E1 in this article's Online Repository at www.jacionline.org). The questionnaire was widely distributed to primary immunodeficiency patients/caregivers through professional organizations (the European Society for Immunodeficiencies, Latin American Society for Immunodeficiencies, and Clinical Immunology Society), patient advocacy groups (the Jeffrey Modell Foundation), and individually to other colleagues by members of the scientific interest group. All data for this retrospective study represented a 10-year cumulative experience for each reporting institution and were collected between April 2010 and March 2012.

Data relevant to (1) SCID diagnosis, treatment, immune reconstitution, and outcome, as well as (2) BCG vaccination and (3) BCG-associated complication diagnosis, treatment, and outcome was analyzed. For the purposes of this multicenter international retrospective study, we analyzed patients given diagnoses of SCID at the participating centers based on the clinical and laboratory findings of recurrent/severe infections and/or failure

TABLE I. BCG-vaccinated patients with SCID: distribution and HSCT

Country (centers)*	Universal BCG vaccination at birth†	BCG-vaccinated patients with SCID (n = 349)	HSCT‡ (n = 190)
Argentina (3)	Yes	10	6
Brazil (3)	Yes	58	24
Colombia (1)	Yes	6	1
Costa Rica (1)	Yes	10	6
Czech Republic (1)§	Yes	15	8
Egypt (1)	Yes	26	1
France (1)	No	44	44
Iran (1)	Yes	31	0
Japan (4)	No	6	6
Kuwait (1)	No	10	4
Mexico (2)	Yes	14	5
Oman (1)	Yes	4	2
Poland (1)	Yes	8	5
Portugal (1)	Yes	5	5
Russia (1)	Yes	8	0
Turkey (3)	No	40	27
United Kingdom (2)	No	54	46

*A total of 821 patients were given diagnoses of SCID in these centers, including 349 who were BCG vaccinated and reported for the current study.
†For recent changes or individualized BCG vaccination policies in different countries, please refer to http://www.bcgatlas.org/.
‡Other forms of SCID treatment (eg, gene therapy, 3 patients; enzyme replacement, 2 patients; or thymus transplantation, 1 patient) are also included in this category.
§National Center Database of Primary Immunodeficiencies, which collects data from 13 centers in the Czech Republic.

to thrive, severe T-cell lymphopenia (in the absence of a condition consistent with Omenn syndrome or maternal engraftment), and/or severe functional T-cell defects. BCG-associated complications were defined based on clinical, microbiological, and/or histopathologic findings and were classified as localized (persistent lesions [ulcer, abscess, fistula, or lymphadenopathy] limited to the region of inoculation) or disseminated (evidence of infection distal to injection-site lesions, including positive blood or bone marrow cultures).[7] Data entered by the referring centers detailing pathologic manifestations that were attributed to an excessive and/or dysregulated immune response to BCG as a consequence of improvement in immune status were associated with a diagnosis of immune reconstitution syndrome (IRS).[8] Deaths caused by BCG-associated complications, as well as all-cause mortality, were analyzed as outcome variables. BCG-associated deaths were defined as cases in which the primary cause of death was strongly associated with BCG-associated complications, as determined by the clinical care team. Continuous variables were compared by using the Kruskal-Wallis test. The Fisher exact test was used to compare proportions. Logistic regression was used to evaluate the effects of covariates on a binary outcome variable. Kaplan-Meier curves were plotted and compared by using the log-rank test. Cox regression was used to evaluate the effects of covariates in a time-to-event analysis. All P values are 2-sided, and P values of less than .05 were considered statistically significant. Data analyses were performed with SAS software (version 9.3; SAS Institute, Cary, NC).

As with any retrospective observational study of this nature, there are limitations that should be considered when interpreting the results. We acknowledge the possibility of diagnostic criteria discrepancies among the participating centers. Our analysis only included children who received BCG vaccinations, and these children might not be representative of the entire SCID population. Because of the limitations of data collection, we used the midpoint of the reported time interval of BCG vaccination and hematopoietic stem cell transplantation (HSCT) in the time-to-event analysis. Additional variability and bias might be introduced by using this *ad hoc* method.

RESULTS

Population demographics

A total of 821 patients were given diagnoses of SCID in the 28 participating centers from 17 different countries, 349 of whom were BCG vaccinated (42%) and analyzed in this retrospective study (Table I). When the analysis was restricted to countries with mandatory at-birth BCG vaccination policies, the rate of BCG-vaccinated patients with SCID increased to 88%.

SCID diagnosis

SCID diagnosis was established in 9% of the patients before the age of 1 month, in 29% before 3 months, in 63% before 6 months, and in 90% before 1 year (Fig 1, *A*). The specific type of SCID diagnosis was determined in 159 (46%) patients and not defined in the remainder of the cohort. *IL2RG* deficiency was the most frequently reported, followed by defects in *RAG1/RAG2*, *ADA*, MHC class II deficiency, *IL7RA*, Artemis *(DCLRE1C)*, Janus kinase 3 *(JAK3)*, purine nucleoside phosphorylase *(PNP)*, zeta chain–associated protein of 70 kDa *(ZAP70)*, and Cernunnos *(NHEJ1)*. We cannot formally exclude that among the patients with no specific SCID type defined, some could have been affected by other known primary immunodeficiency diseases presenting with an SCID-like phenotype of severe T-cell lymphopenia and/or severe functional T-cell defects and increased susceptibility to mycobacterial diseases (eg, Mendelian susceptibility to mycobacterial disease–associated genetic defects).

BCG vaccination

Age at vaccination was determined in 345 of 349 patients with SCID. The majority (258/345 [75%]) were vaccinated within the first month of life (<1 week, 204 patients; 1-2 weeks, 6 patients; and 3-4 weeks, 48 patients), whereas the remainder (87/345) were vaccinated later (1-3 months, 74 patients; 4-6 months, 8 patients; 7-12 months, 3 patients; and >12 months, 2 patients). BCG vaccine was administrated on the deltoid area in all patients: 301 intradermally, 38 subcutaneously, and 10 in an undetermined manner. The vaccine strain was reported in 252 patients: Danish, 88 patients; Moreau, 66 patients; Pasteur, 32 patients; Glaxo, 29 patients; Tokyo, 19 patients; and Russia, 18 patients.

BCG-associated complications

BCG-associated complications are described in Fig 1, *B* to *F*. After BCG vaccination, 177 (51%) patients with SCID had complications: 59 (17%) localized and 118 (34%) disseminated, a 400- and 33,000-fold increase, respectively, over the general population. Age at onset of BCG-associated complications was determined in 158 patients: less than 1 month in 8 patients, 1 to 3 months in 33 patients, 4 to 6 months in 67 patients, 7 to 12 months in 34 patients, and greater than 12 months in 16 patients. Among patients presenting with disseminated complications, involvement of the extraregional lymph nodes (n = 67 [57%]), skin (n = 66 [56%]), or lungs (n = 55 [47%]) was the most common clinical presentation; BCG infections compromising the liver (n = 18 [15%]), spleen, and bones (n = 15 [13% each]) were reported less frequently. Isolation of *M bovis* BCG from bone marrow was described in 14% (n = 17) of patients with disseminated complications, whereas positive blood culture results were even more uncommon (n = 1 [1% of patients with disseminated complications]).

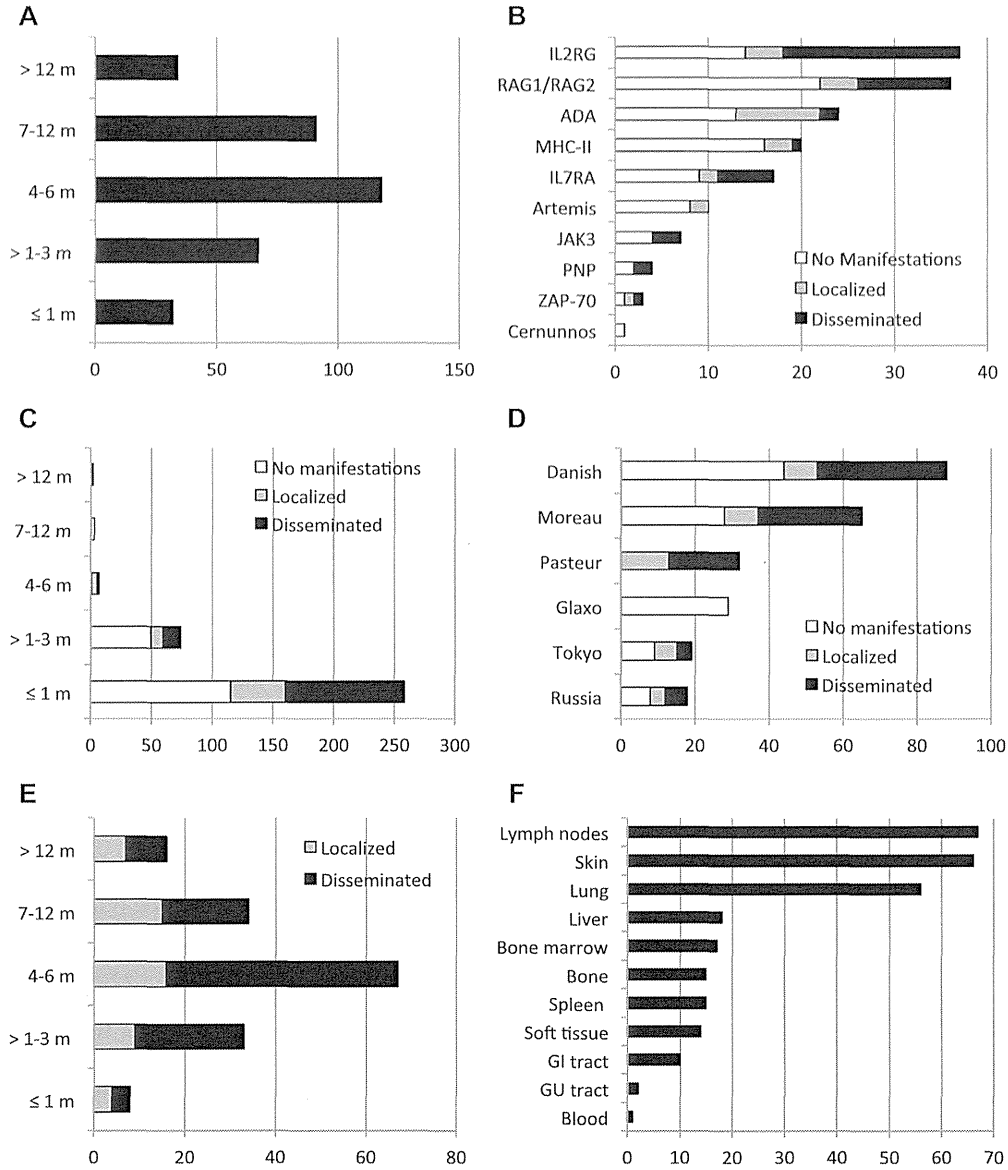

FIG 1. BCG-vaccinated patients with SCID: epidemiologic characteristics. **A,** Age at SCID diagnosis. **B,** SCID diagnosis and BCG-associated complications (no manifestations or localized or disseminated complications). **C,** Age at BCG vaccination and BCG-associated complications (no manifestations or localized or disseminated complications) distribution. **D,** BCG vaccine strain and BCG-associated complications (no manifestations or localized or disseminated complications). **E,** Age at onset of BCG-associated complications (localized or disseminated complications). **F,** Site of involvement of disseminated BCG-associated complications. *GI,* Gastrointestinal; *GU,* genitourinary. *X-axis,* number of patients.

The median absolute T-cell number at the time of SCID diagnosis in patients with localized or disseminated BCG-associated complications was significantly lower than that in patients without BCG-associated complications ($P = .003$, Table II). Logistic regression analysis showed that the odds of experiencing BCG-associated complications among patients with SCID with T-cell numbers of 250/μL or less at diagnosis was 2.1 times higher (95% CI, 1.4-3.4 time higher; $P = .001$) than that among those with T-cell numbers of greater than 250/μL, and the difference remained significant after adjusting for the age at BCG vaccination. Patients with and without BCG-associated complications were not significantly different in either B-cell or natural killer cell numbers.

Two hundred thirty-eight (68%) patients received antimycobacterial treatment after receiving a diagnosis of SCID. At the time of treatment initiation, 78 (22%) were asymptomatic in terms of BCG-associated complications, and 160 (46%) were symptomatic (53 with localized and 107 with disseminated manifestations).

Among asymptomatic antimycobacterial agent–treated patients who underwent HSCT (n = 64), 49 (77%) received multidrug antimycobacterial therapy (MAT), whereas 10 (16%) were treated with isoniazid monotherapy (no information on 5 patients). MAT included isoniazid plus rifampicin–based treatment in 49 (77%) patients, 18 of them (28%) having 1 or more additional drugs. The enteral route was preferred in 94% of these

TABLE II. BCG-vaccinated patients with SCID: statistical analysis

Age at BCG vaccination			
	BCG vaccination at ≤1 mo	BCG vaccination at >1 mo	*P* value
Sex, no. (%)			
Female	88 (34.8)	40 (46)	NS
Male	165 (65.2)	47 (54	
Age at SCID diagnosis (mo), median (range)	5 (0.5-48)	6 (0.5-100)	NS
BCG-associated complications, no. (%)			
No manifestations	115 (44.6)	54 (62.1)	.006
Loc/Diss manifest	143 (55.4)	33 (37.9)	
Age at HSCT (mo), median (range)	7 (0.5-75)	8 (0.5-107)	NS
Mortality in BCG-SCID			
BCG-rel, no. (%)	45 (18)	0 (0)	<.0001
Overall, no. (%)	132 (52.8)	38 (43.7)	NS

Median lymphocytes at SCID diagnosis			
	No manifestations	Localized or disseminated	
T cells/μL (25th-75th percentile)	197 (14-942)	49 (5-343)	.003
B cells/μL (25th-75th percentile)	103 (5-640)	140 (11-710)	NS
NK cells/μL (25th-75th percentile)	160 (38-410)	100 (19-366)	NS

BCG-rel, Death related to BCG-associated complications; *Loc/Diss manifest*, localized or disseminated manifestations of BCG-associated complications; *NK*, natural killer; *No manifestations*, no manifestations of BCG-associated complications; *NS*, not significant.

patients. No significant differences between monotherapy and MAT were detected when death caused by BCG-associated complications was compared ($P = .99$). By the time of data analysis, 63% of these patients were alive (median follow-up, 57 months; range, 4-126 months). Among symptomatic patients receiving antimycobacterial treatment and undergoing HSCT (n = 76), 64 (82%) were treated with MAT, whereas 4 (5%) were treated with isoniazid monotherapy (no information on 8 patients). MAT included isoniazid plus rifampicin–based treatment in 61 (80%) patients, 47 (62%) of them having 1 or more drugs added to the scheme. Eighty-four percent of these patients were treated through the enteral route, and 11% were treated through a mixed (enteral and parenteral) route. By the time of data analysis, 70% of these patients were alive (median follow-up, 45 months; range, 0-158 months).

BCG-associated complications were reported in 3% (2/64) of asymptomatic patients receiving antimycobacterial treatment and undergoing HSCT. Antimycobacterial treatment of already symptomatic patients undergoing HSCT resulted in complete clinical resolution of the infection in 30%, partial resolution in 46%, and no resolution in 24%. After HSCT, 59% of the patients were kept on antimycobacterial treatment: 32% for less than 3 months, 15% for 4 to 6 months, 21% for 7 to 12 months, and 32% for more than a year.

No deaths related to BCG-associated complications were reported among BCG-asymptomatic treated patients with SCID, whereas 46 deaths caused by BCG occurred among BCG-symptomatic treated patients (7 in patients who underwent HSCT and 39 in patients who did not, including 45 patients with disseminated complications and 1 patient with localized disease; $P < .0001$). The median age of death for these patients (38 with reported data) was 6.8 months. When the analysis was restricted to patients undergoing HSCT, no deaths were reported among the asymptomatic treated group (0/64), and 7 deaths occurred among the 120 symptomatic treated patients ($P = .09$).

One hundred eleven BCG-vaccinated patients with SCID (32%; 96 of them presenting with no manifestations and 15 symptomatic, including 9 with disseminated and 6 with localized complications) did not receive antimycobacterial treatment after SCID diagnosis. Forty-five (40%) of these patients underwent HSCT (32 asymptomatic and 13 symptomatic, including 8 with disseminated and 5 with localized complications), 15 of them received antimycobacterial treatment after HSCT (3 asymptomatic and 8 with disseminated and 4 with localized manifestations), 28 of them (63%) are alive, and no deaths caused by BCG-associated complications were reported (median follow-up, 46 months; range, 0-187 months). Of the remaining 66 patients (60%, 64 were asymptomatic and 2 were symptomatic, including 1 with disseminated and 1 with localized complications) who did not undergo HSCT by the time of data analysis, 22 (33%) were alive, and only 1 BCG-associated death was reported in this group (presenting with disseminated disease). Interestingly, survival rates for patients who did not receive pre-HSCT antimycobacterial treatment (27/45) was not statistically different from those in patients who received antimycobacterial treatment and underwent HSCT (94/139, $P = .47$).

Age at BCG vaccination showed a significant association with BCG-associated complications independently of the type of SCID, the vaccine strain, or the route of vaccination. Patients vaccinated within the first month of life showed an increased prevalence of BCG-associated complications (disseminated or localized) compared with patients vaccinated after 1 month of age ($P = .006$). Moreover, the odds of having BCG-associated complications among those vaccinated within the first month of life were 2.03 times higher than those vaccinated after the age of 1 month (odds ratio, 2.03; 95% CI, 1.24-3.35). A log-rank test comparing time to death caused by BCG-associated complications in patients vaccinated within or after 1 month of age also identified significant differences between these 2 groups ($P < .0001$, Fig 2). Moreover, survival analysis comparing time to death within 24 months of age before HSCT for patients vaccinated early versus late showed that the hazard of death was 2.12 times higher for those receiving early vaccination (95% CI, 1.12-3.89; Fig 2). These results strongly suggested that early BCG vaccination (≤1 month) is associated with increased BCG-associated complications and subsequent death associated with those complications.

SCID treatment

Of the 349 BCG-vaccinated patients with SCID, 190 (54%) underwent HSCT (n = 184) or another form of SCID-specific treatment (eg, gene therapy [n = 3], enzyme replacement [n = 2], or thymus transplantation [n = 1]). The median age at HSCT was 7.5 months (range, 0.5-107 months). No significant differences in T-cell engraftment were detected between patients receiving early (≤1 month) versus late (>1 month) BCG vaccination or among patients undergoing transplantations without or with BCG-associated complications (localized or disseminated). No significant differences in the proportion of death caused by

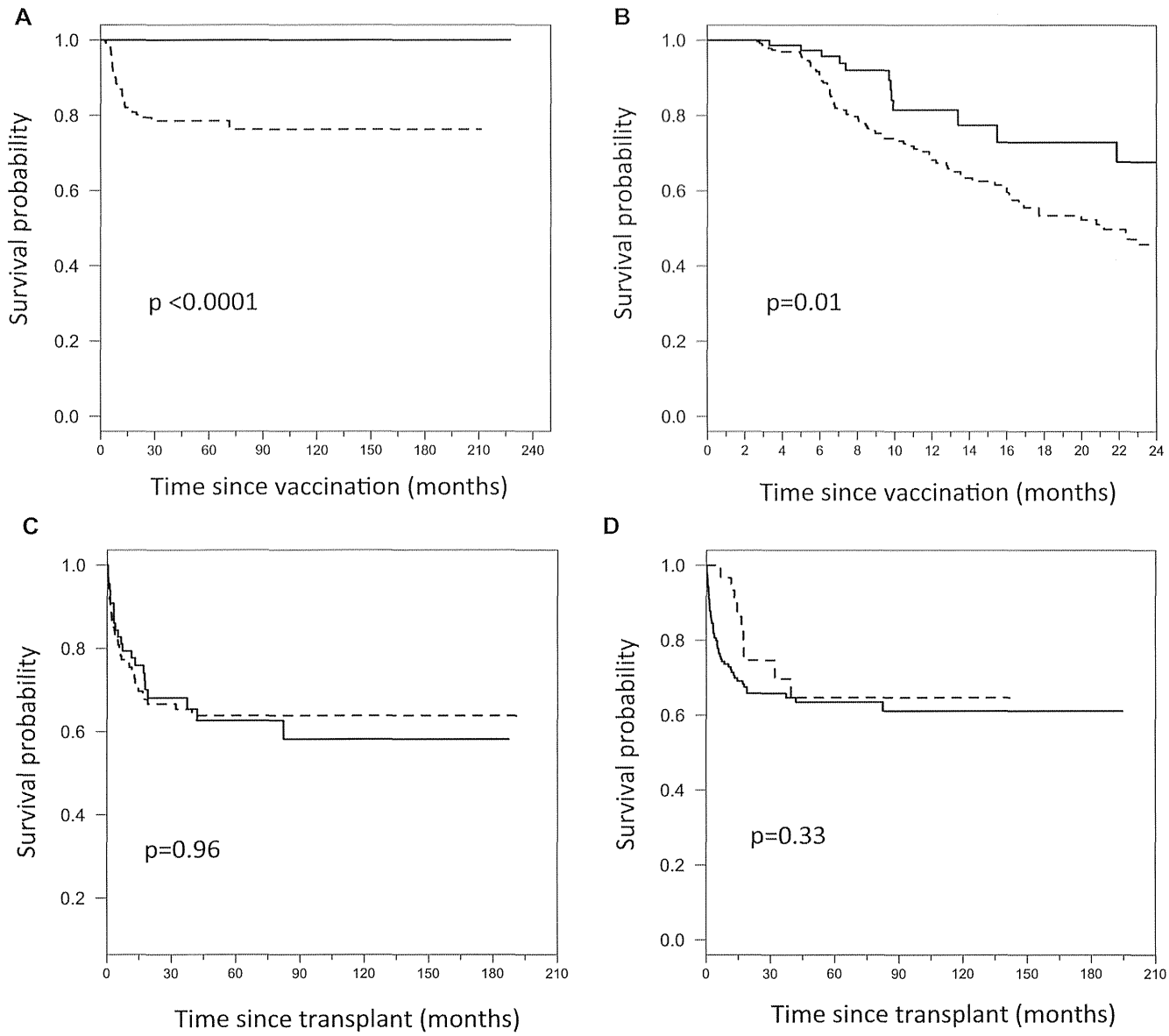

FIG 2. Time-to-event analysis by age at BCG vaccination and age at HSCT. **A,** Kaplan-Meier curves for the time from vaccination to death caused by BCG-associated complications comparing early (≤1 month of age, *dashed line*) versus late (>1 month of age, *solid line*) vaccination ($P < .0001$). **B,** Kaplan-Meier curves for the time from vaccination to death within 24 months of age before HSCT comparing early (≤1 month of age, *dashed line*) versus late (>1 month of age, *solid line*) vaccination ($P = .01$). **C,** Kaplan-Meier curves for time from HSCT to death comparing early (≤1 month of age, *dashed line*) versus late (>1 month of age, *solid line*) vaccination ($P = .96$). **D,** Kaplan-Meier curves for the time from HSCT to death comparing early (≤3 months of age, *dashed line*) versus late (>3 months of age, *solid line*) transplantation ($P = .33$).

BCG-associated complications were detected either among patients receiving matched related, matched unrelated, mismatched related, or mismatched unrelated forms of HSCT ($P = .97$). However, death caused by BCG-associated complications was still more frequent among patients receiving early vaccination compared with those vaccinated later ($P = .049$). Death caused by BCG-associated complications was also significantly more frequent among patients undergoing HSCT with localized or disseminated BCG-associated complications versus those with no manifestations ($P = .006$). When all-cause mortality was compared among patients receiving HSCT, no significant difference was detected between patients receiving early versus late BCG vaccination ($P = .96$), implying that after HSCT, the age at BCG vaccination has no significant effect on survival rates (Fig 2). Finally, although we did not find significant differences in post-HSCT survival between early (≤3 months) and late (>3 months) HSCT ($P = .33$), the difference between these 2 groups within the first 12 months after transplantation was statistically significant ($P = .01$, Fig 2).

Of 190 patients who underwent HSCT or another form of SCID treatment, 55 (29%) had IRS (33 with disseminated disease, 14 with localized complications, and 8 with no manifestations). Most patients (57%) presented with these manifestations within a month of HSCT. IRS prevalence was also analyzed in different

subsets of patients: those receiving antimycobacterial treatment while BCG asymptomatic had significantly less of this complication (5/64) compared with either BCG-symptomatic antimycobacterial-treated patients (33/81, $P < .0001$) or nontreated patients (17/45, $P = .0003$).

DISCUSSION

The prevalence of BCG-associated complications in the general population can vary widely depending on the reporting country and the vaccine strain used. However, reports of 1 in 2,500 vaccinees presenting with localized BCG-associated complications and 1 in 100,000 presenting with disseminated complications represent a fair estimate of the prevalence of such complications.[1,9] When focused exclusively on patients given a diagnosis of SCID, the prevalence of BCG-associated complications has been estimated to be higher than in the general population,[10-12] although a definitive effect has not previously been established.

The cumulative experience of 28 centers in 17 countries from Africa, the Americas, Asia, and Europe confirms that, as expected, BCG-associated complications are more prevalent in patients with SCID than in the general population. On the basis of our observations, one in every 2 BCG-vaccinated patients with SCID had BCG-associated manifestations, two thirds in the form of disseminated complications (an approximate 33,000-fold increased compared with the general population) and the other third in the form of localized complications (an approximate 400-fold increase). Our analysis found 2 individual variables to significantly correlate with this increased prevalence of BCG-associated complications: the total number of T cells at the time of SCID diagnosis and the patient's age at the time of BCG vaccination. Although patients with SCID presenting with higher T-cell numbers were underrepresented among those with BCG-associated complications, these results should be cautiously interpreted. Maternal T-cell engraftment was not systematically evaluated in most of the patients surveyed, and patients presenting with Omenn syndrome and oligoclonal T-cell expansion were not excluded from the analysis. Furthermore, detailed information on T-cell functional studies were not part of the original survey and analysis. On the other hand, age at BCG vaccination appeared to be a strong predictor for BCG-associated complications, with patients vaccinated within the first month of life having a substantially higher risk, which in turn was also associated with an increased rate of death caused by vaccine-associated complications. Age at BCG vaccination was independent of other variables, including BCG strain, vaccination route, or type of SCID diagnosed. Less clear than the association between age of vaccination and complications are the mechanism or mechanisms underlying this finding. All patients with SCID, independent of their underlying genetic defect, share a defective adaptive immune response. Therefore the relative maturity of the innate immune arm involved with controlling mycobacterial infections could by hypothesized as a factor altering the balance toward controlling or not controlling BCG.[13,14] Equally as relevant as determining the biological mechanism to explain this variability is developing a strategy to intervene and improve the clinical outcome.

BCG vaccine has a worldwide coverage of 88% (http://apps.who.int/immunization_monitoring/en/globalsummary/GS_GLOProfile.pdf?CFID=6942726&CFTOKEN=73185195), and most of these vaccines are applied at birth (http://www.bcgatlas.org/). Similar to other large SCID series published,[15,16] the majority of patients in our cohort (63%) were given diagnoses of SCID within the first 6 months of life. Until safer and more efficient forms of antituberculosis vaccines become available,[17] delaying BCG vaccination beyond 1 month of age is likely to have a favorable effect in this highly vulnerable population, as well as other susceptible neonates (eg, HIV-positive infants).[18] Moreover, delaying BCG vaccination would also benefit the clinical effect of neonatal SCID screening, preventing application of an absolutely contraindicated vaccine before establishing the diagnosis of SCID. This issue will become increasingly relevant as countries still encouraging early BCG vaccination start implementing neonatal SCID screening.[19,20]

However, 2 major drawbacks could be foreseen in delaying BCG vaccination: the "missed opportunity" of vaccinating patients after birth based on the concept that there will be an associated decrease in coverage and the potential increased risk of BCG-preventable diseases during the "unprotected" intervals. WHO data (updated to July 12, 2012) demonstrated a BCG coverage of 89.2% for countries encouraging at-birth vaccination policies, values that are very similar to the 89% coverage in the same countries for administration of the third dose of diphtheria-pertussis-tetanus vaccine (DPT3) typically given at 6 months of age (http://apps.who.int/immunization_monitoring/en/globalsummary/timeseries/tscoveragedtp3.htm). These data suggest there would be little or no decrease in coverage by delaying BCG vaccination. In addition, the incidence of BCG-preventable mycobacterial diseases within the first 6 months of life is extremely uncommon. Literature on pediatric tuberculous meningitis, a BCG vaccine–preventable disease, shows that the mean age of presentation for this life-threatening disease is 23 to 49 months, although a few cases have been described during the first 6 months of life, whereas the medians span from 12 to 24 months of age.[21-26] The prospect of modifying BCG vaccination policies will certainly warrant extensive discussions balancing the needs of both the immunocompetent general population and highly vulnerable immunodeficient patients.

As expected, the major intervention affecting survival in this cohort of BCG-vaccinated patients with SCID was providing immunologic reconstitution by means of HSCT. Interestingly, a subset of patients who did not receive any antimycobacterial treatment but underwent HSCT did not have any BCG-associated complications or IRS (27/190). This outcome might suggest that HSCT by itself could suffice as an anti-BCG treatment; however, other variables could have potentially influenced these results, including vaccine viability,[27] SCID genotype (13 undefined SCIDs, 7 MHC class II deficiency, 2 *IL2RG*, 1 *JAK3*, 1 Artemis *(DCLRE1C)*, 1 *PNP*, 1 *IL7RA*, and 1 Cernunnos *(NHEJ1)*; median T-cell numbers, 250/μL; median age at HSCT, 7 months), higher maturity of innate immunity, residual acquired immunity, or other unidentified disease modifiers.

We observed that patients with SCID started on antimycobacterial therapy while BCG-asymptomatic had significantly fewer BCG-associated complications before HSCT, as well as less IRS after HSCT and decreased mortality caused by BCG-associated complications. The rationale for this approach is to control an infection involving the known inoculation of 37,500 to 3,200,000 live mycobacteria in a highly susceptible host.[28] However, we recognize that our data do not provide definitive proof of benefit for pre-emptive antimycobacterial therapy because of

confounding factors associated with this type of retrospective study. Still, in the setting of commonly used prophylactic therapy in patients with SCID (eg, immunoglobulin replacement and antimicrobial agents), it seems entirely appropriate to consider early initiation of antimycobacterial therapy at the time of SCID diagnosis. If this strategy is chosen, it is less clear which antimycobacterial scheme would be most effective.

In summary, our data strongly suggest that in patients with SCID, early BCG vaccination and lower T-cell numbers at SCID diagnosis increase the probability of having BCG-associated complications. Furthermore, patients with SCID presenting with BCG-associated complications are at increased risk of dying because of this. Finally, the age at BCG vaccination had no significant influence on survival rates in patients with SCID who received HSCT.

We thank all the patients, their families, and the medical teams who took and take care of our patients. We also thank the IT Department of the Hospital Garrahan in Buenos Aires, Argentina, for generating a Web site for the survey, and Dr Klaus Warnatz for his help and support with the logistics of the survey.

Clinical implications: Delaying BCG vaccination until after 1 month of age should diminish BCG-associated complications in patients with SCID and should not adversely affect BCG-preventable disease.

REFERENCES

1. Plotkin SA, Orenstein WA, Offit PA. *Vaccines*. 6th ed. Edinburgh: Elsevier/Saunders; 2013.
2. Comstock GW. The International Tuberculosis Campaign: a pioneering venture in mass vaccination and research. Clin Infect Dis 1994;19:528-40.
3. Fine PE. Bacille Calmette-Guerin vaccines: a rough guide. Clin Infect Dis 1995; 20:11-4.
4. Buckley RH. Transplantation of hematopoietic stem cells in human severe combined immunodeficiency: longterm outcomes. Immunol Res 2011;49:25-43.
5. Al-Herz W, Bousfiha A, Casanova JL, Chapel H, Conley ME, Cunningham-Rundles C, et al. Primary immunodeficiency diseases: an update on the classification from the international union of immunological societies expert committee for primary immunodeficiency. Front Immunol 2011;2:54.
6. General recommendations on immunization—recommendations of the Advisory Committee on Immunization Practices (ACIP). MMWR Morb Mortal Wkly Rep 2011;60:1-64.
7. Talbot EA, Perkins MD, Silva SF, Frothingham R. Disseminated Bacille Calmette-Guerin disease after vaccination: case report and review. Clin Infect Dis 1997;24: 1139-46.
8. Gantzer A, Neven B, Picard C, Brousse N, Lortholary O, Fischer A, et al. Severe cutaneous bacillus Calmette-Guerin infection in immunocompromised children: the relevance of skin biopsy. J Cutan Pathol 2013;40:30-7.
9. Lotte A, Wasz-Hockert O, Poisson N, Engbaek H, Landmann H, Quast U, et al. Second IUATLD study on complications induced by intradermal BCG-vaccination. Bull Int Union Tuberc Lung Dis 1988;63:47-59.
10. Romanus V, Fasth A, Tordai P, Wiholm BE. Adverse reactions in healthy and immunocompromised children under six years of age vaccinated with the Danish BCG vaccine, strain Copenhagen 1331: implications for the vaccination policy in Sweden. Acta Paediatr 1993;82:1043-52.
11. Gonzalez B, Moreno S, Burdach R, Valenzuela MT, Henriquez A, Ramos ML, et al. Clinical presentation of Bacillus Calmette-Guerin infections in patients with immunodeficiency syndromes. Pediatr Infect Dis J 1989;8:201-6.
12. Yao CM, Han XH, Zhang YD, Zhang H, Jin YY, Cao RM, et al. Clinical characteristics and genetic profiles of 44 patients with severe combined immunodeficiency (SCID): report from Shanghai, China (2004-2011). J Clin Immunol 2013; 33:526-39.
13. Sharma AA, Jen R, Butler A, Lavoie PM. The developing human preterm neonatal immune system: a case for more research in this area. Clin Immunol 2012;145: 61-8.
14. Satwani P, Morris E, van de Ven C, Cairo MS. Dysregulation of expression of immunoregulatory and cytokine genes and its association with the immaturity in neonatal phagocytic and cellular immunity. Biol Neonate 2005;88:214-27.
15. Buckley RH, Schiff RI, Schiff SE, Markert ML, Williams LW, Harville TO, et al. Human severe combined immunodeficiency: genetic, phenotypic, and functional diversity in one hundred eight infants. J Pediatr 1997;130:378-87.
16. Gennery AR, Slatter MA, Grandin L, Taupin P, Cant AJ, Veys P, et al. Transplantation of hematopoietic stem cells and long-term survival for primary immunodeficiencies in Europe: entering a new century, do we do better? J Allergy Clin Immunol 2010;126:602-10, e601-11.
17. Parida SK, Kaufmann SH. Novel tuberculosis vaccines on the horizon. Curr Opin Immunol 2010;22:374-84.
18. Koppel A, Leonardo-Guerrero J, Rives S, Paniagua-Torres N, Sparrow C, Beck-Sague CM. Immune reconstitution inflammatory syndrome due to *Mycobacterium bovis* Bacillus Calmette-Guerin in infants receiving highly active antiretroviral therapy: a call for universal perinatal rapid HIV testing prior to administration of BCG immunization of neonates. J Trop Pediatr 2010;56:280-3.
19. Chien Y-H, Chiang S-C, Chang K-L, Yu H-H, Lee W-I, Tsai L-P, et al. Incidence of severe combined immunodeficiency through newborn screening in a Chinese population. J Formosan Med Assoc [Epub ahead of print].
20. Kanegae MPP, dos Santos AMN, Cavalcanti CM, Condino Neto A. Newborn screening for severe combined immunodeficiency. Rev Brasil Alerg Immunopatol 2011;34:1-7.
21. van Well GT, Paes BF, Terwee CB, Springer P, Roord JJ, Donald PR, et al. Twenty years of pediatric tuberculous meningitis: a retrospective cohort study in the western cape of South Africa. Pediatrics 2009;123:e1-8.
22. Lee LV. Neurotuberculosis among Filipino children: an 11 years experience at the Philippine Children's Medical Center. Brain Dev 2000;22:469-74.
23. Farinha NJ, Razali KA, Holzel H, Morgan G, Novelli VM. Tuberculosis of the central nervous system in children: a 20-year survey. J Infect 2000;41:61-8.
24. Yaramis A, Gurkan F, Elevli M, Soker M, Haspolat K, Kirbas G, et al. Central nervous system tuberculosis in children: a review of 214 cases. Pediatrics 1998;102: E49.
25. Doerr CA, Starke JR, Ong LT. Clinical and public health aspects of tuberculous meningitis in children. J Pediatr 1995;127:27-33.
26. Paganini H, Gonzalez F, Santander C, Casimir L, Berberian G, Rosanova MT. Tuberculous meningitis in children: clinical features and outcome in 40 cases. Scand J Infect Dis 2000;32:41-5.
27. Ho MM, Markey K, Rigsby P, Jensen SE, Gairola S, Seki M, et al. Report of an international collaborative study to establish the suitability of using modified ATP assay for viable count of BCG vaccine. Vaccine 2008;26:4754-7.
28. Milstien JB, Gibson JJ. Quality control of BCG vaccine by WHO: a review of factors that may influence vaccine effectiveness and safety. B World Health Organ 1990;68:93-108.

SCIENTIFIC REPORTS

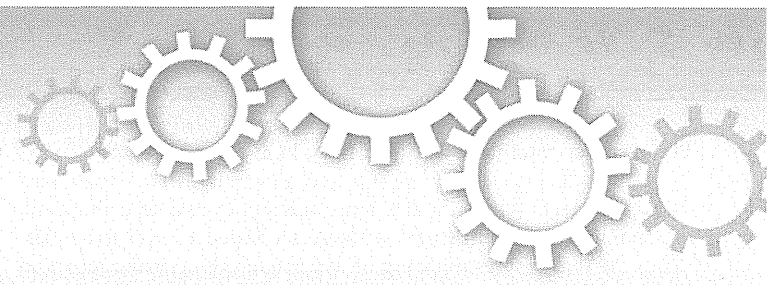

OPEN

SUBJECT AREAS:
CELL DEATH AND IMMUNE RESPONSE
LAB-ON-A-CHIP
SINGLE-CELL IMAGING
CELLULAR IMAGING

Received
3 October 2013

Accepted
2 April 2014

Published
22 April 2014

Correspondence and requests for materials should be addressed to O.O. (oosamu@rcai.riken.jp)

Real-time single-cell imaging of protein secretion

Yoshitaka Shirasaki[1], Mai Yamagishi[1], Nobutake Suzuki[1], Kazushi Izawa[2], Asahi Nakahara[3], Jun Mizuno[3], Shuichi Shoji[3], Toshio Heike[2], Yoshie Harada[4], Ryuta Nishikomori[2] & Osamu Ohara[1,5]

[1]RIKEN Center for Integrative Medical Sciences (IMS-RCAI), 1-7-22 Suehiro-cho Tsurumi-ku, Yokohama, Kanagawa 230-0045, Japan, [2]Department of Pediatrics, Kyoto University Graduate School of Medicine, 54 Shogoin-Kawahara-cho Sakyo-ku, Kyoto 606-8507, Japan, [3]Faculty of Science and Engineering, Waseda University, Okubo 3-4-1, Shinjuku, Tokyo 169-8555, Japan, [4]Institute for Integrated Cell-Material Sciences (WPI-iCeMS), Kyoto University Graduate School of Biostudies, Yoshida-Honmachi, Sakyo-ku, Kyoto 606-8501, Japan, [5]Department of Human Genome Research, Kazusa DNA Research Institute, 2-6-7 Kazusa-Kamatari, Kisarazu, Chiba 292-0818, Japan.

Protein secretion, a key intercellular event for transducing cellular signals, is thought to be strictly regulated. However, secretion dynamics at the single-cell level have not yet been clarified because intercellular heterogeneity results in an averaging response from the bulk cell population. To address this issue, we developed a novel assay platform for real-time imaging of protein secretion at single-cell resolution by a sandwich immunoassay monitored by total internal reflection microscopy in sub-nanolitre-sized microwell arrays. Real-time secretion imaging on the platform at 1-min time intervals allowed successful detection of the heterogeneous onset time of nonclassical IL-1β secretion from monocytes after external stimulation. The platform also helped in elucidating the chronological relationship between loss of membrane integrity and IL-1β secretion. The study results indicate that this unique monitoring platform will serve as a new and powerful tool for analysing protein secretion dynamics with simultaneous monitoring of intracellular events by live-cell imaging.

Many secreted proteins have been identified as important functional mediators of intercellular communication for the purpose of initiating various cellular processes, including differentiation and migration[1–3]. Cytokines in particular are one of the best studied classes of secreted proteins with broad effects on immune responses[4]. For the proper functioning of the immune system, cytokine synthesis and secretion must be tightly regulated, both spatially and temporally[5]. However, recent investigations using single-cell analysis have shown that immune cells display highly heterogeneous levels of cytokine secretion, even in cells with apparently similar phenotypes[6]. Therefore, the relationship between heterogeneous cytokine secretion at the single-cell level and the maintenance of homeostasis of the immune system has become a primary subject of investigation in the field of immunology. To address this issue, a methodology is required that enables delineation of spatiotemporal heterogeneity of cytokine secretion at the single-cell level. We have particularly focused on cytokine induction processes that occur in single cells induced by external stimulation, specifically with regard to (1) cellular heterogeneity in protein secretion dynamics and (2) the chronological relationship between intracellular event(s) and protein secretion. However, the technology available for monitoring protein secretion from single cells remains in its infancy.

Several groups have reported population analysis of cytokine secretion from single cells by using antibody-based immunoassay applications. Love *et al.* generated a secretion profile for a large collection of single cells by using microengraving[7] and succeeded in measuring the time course of cytokine secretion during T-lymphocyte maturation every 2 h for a period spanning several hours[8]. While these methods are efficient for their high throughput and/or the quantitative data generated, several challenges remain because of their inherent measurement limitations. In these methods, the accumulated cytokine molecules situated on a solid surface are labelled with a detection probe and are quantified after intensive wash steps, which are required to remove excess probe. Although this wash step, known as bound/free (B/F) separation, determines the signal/noise ratio for detection, this step also causes a lag between secretion and detection. Therefore, these methods cannot currently offer either a time interval of shorter than a few hours nor simultaneous real-time monitoring of a second intracellular variable (e.g. cell viability) over time.

Previously, our group and Salehi-Reyhani *et al.* respectively have successfully addressed this B/F separation issue in fluorescence immunoassays (FIAs) by taking advantage of near-field excitation in total internal reflection

fluorescence microscopy (TIRFM)[9,10]. In these studies, target proteins in each single-cell lysate segmented by microwells were quantified by detecting formation of immunocomplexes on the microwell bottom. In the current study, we have developed a novel assay platform for real-time monitoring of live single-cell cytokine secretion (Fig. 1). Each single cell is deposited on a microfabricated-well array (MWA) chip, which restricts cell migration as well as compartmentalizes the secretory signals from individual cells. The anti-cytokine capture antibody immobilized on the microwell bottom immediately captures the cytokine secreted from a cell, which enables TIRFM-FIA to function *in situ*. An MWA chip of the platform has an open architecture at the top of each microwell to permit easy access for stimulus delivery and to maintain culture conditions similar to those of a bulk experiment.

We characterized our secretion assay platform using a MWA chip consisting of glass and polydimethylsiloxiane (PDMS) in a quantitative manner by model experiments, introducing minute amounts of cytokine into microwells to mimic the milieu of cytokine secretion from a single cell. The platform was applied to monitor cytokine secretion from human peripheral blood monocytes at 1-min time intervals. We examined the IL-1β secretion process while simultaneously observing membrane integrity to determine the intracellular processes that occur at the time of cytokine secretion, since the mechanism underlying the non-classical IL-1β secretion pathway currently remains unclear.

Results

Characterization of an assay platform for real-time secretion imaging in an MWA chip. In this study, we designed a real-time single-cell imaging platform to monitor the secretion processes over time. We fabricated a novel MWA chip consisting of a PDMS well wall and a glass well bottom (see Supplementary Fig. S1a online). An objective of numerical aperture 1.49 was used to avoid the stray light due to the higher refractive index of PDMS (n = 1.42, Sylgard®184, Dow Corning Co., http://www1.dowcorning.com/DataFiles/090007c8803bb6a1.pdf) than that of medium (n = 1.34; Supplementary Fig. S1b–d). To assess restriction of the horizontal movement of secreted cytokine molecules by the microwell structure, we compared the decrease of fluorescently labelled protein from an observation area for TIRFM with and without microwell structures. The microwell structure slowed the escape of fluorescent molecules by about 20-fold (see Supplementary Fig. S2).

Next, to assess the functionality of time-resolved FIA (even in the open MWA), we introduced a miniscule amount of cytokine into microwells by using a microinjector to mimic cytokine secretion from a single cell (Fig. 2a). Fluorescence signals began to increase immediately after pulsed injection of IL-1β (time = 0; Fig. 2b, c) and increased without apparent change in localization over time (Fig. 2b), indicating that most of the injected IL-1β was instantly captured by antibody on the MWA bottom before diffusion throughout the microwell. From a separate experiment, we found that the fluorescence signals after the injection of pre-formed IL-1β-detection antibody complexes increased 15 times faster than that after the injection of IL-1β alone, suggesting that the released IL-1β rapidly bound to the capture antibodies on the bottom surface of the MWA chip (Fig. S3a, b). Therefore, binding of the detection antibody to form sandwich immunocomplexes was likely the rate-limiting step for the increase in the fluorescence signals under the experimental conditions employed. Once the immunocomplex was formed, its dissociation occurred very slowly (dissociation constant $k_{off} < 2 \times 10^{-6}$ s^{-1}, Fig. S3c).

The rising curves of the fluorescence signal obtained from IL-1β injection were fitted with a single exponential, especially during

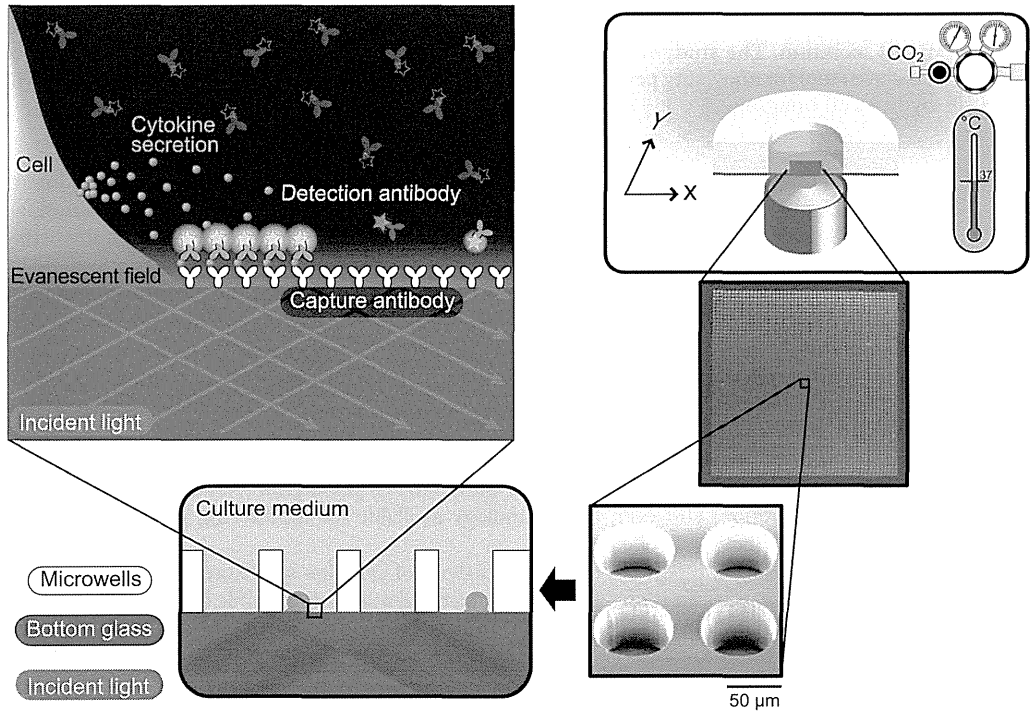

Figure 1 | Concept of the real-time single cell secretion assay platform. The schematic illustrates the concept of the platform for the real-time single cell secretion assay. The platform works with micro-fabricated well-array chip on a fully automated fluorescence microscopy. The platform maintains the environment (temperature, concentration of CO_2, and humidity) of the chip. The chip has an array of nanolitre-sized microwells with a glass bottom, into which individual cells were introduced separately. The well has open-ended structure; therefore, culture medium was exchanged constantly during the observation. The anti-cytokine capture antibody was immobilized on the well bottom, onto which secreted cytokine and fluorescently labelled detection antibody were bound to form a sandwich immunocomplex. Near-field excitation by total internal reflection enabled selective detection of the cytokine sandwich immunocomplex immediately following secretion without the requirement for wash steps.

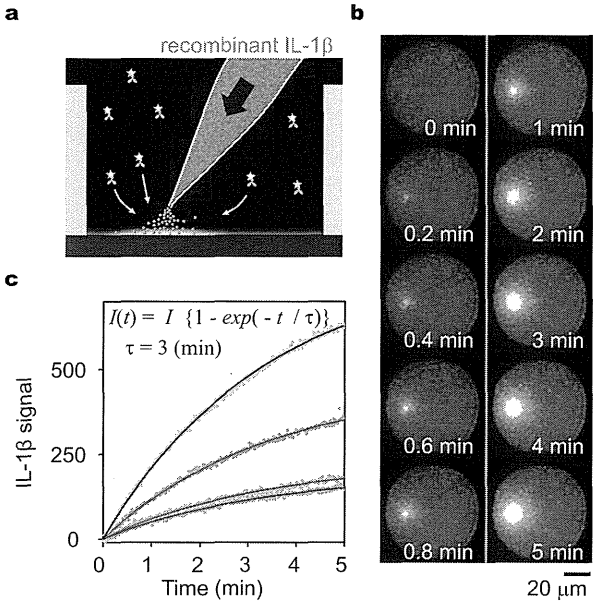

Figure 2 | Performance evaluation of time-resolved FIA in the MWA on model experiments using a microinjector. (a) Schema of the model experiment using pulsed injection of IL-1β via a microinjector. An increase in fluorescence signal was observed after pulse injecting 100 ng/mL of recombinant IL-1β into a microwell that was filled with the detection medium containing 30 nM fluorescently labelled detection antibody. (b) Representative images of developing fluorescence signals obtained from time-resolved FIA after introducing recombinant IL-1β into the microwell. Images were acquired once every second applying a 60-ms exposure time. The time elapsed after the pulsed injection is shown on each image. (c) Time course of the average intensity of the IL-1β signal in a microwell. Each dot denotes a measured value and solid lines denote fitted curves. Different colours denote different durations under a constant pressure of injection (1,200 Pa): 4 s (black), 2 s (green), 0.5 s (blue), and 0.1 s (cyan). Curve fitting was performed for every dataset from 0 to 5 min using the global parameter of time constant, τ, and local parameters of maximum intensity, I, and consequently τ was determined as 3 min.

5 min after injection, and the time constant was estimated to be 3 min (Fig. 2c). Using this parameter, we evaluated the accuracy for determination of the onset time by fitting a single exponential to the dataset quantifying the fluorescence increase obtained within an arbitrary time interval. The accuracy of computed onset time was determined within 0.1 min when using a dataset with 1-min time intervals (Fig. S4).

The increase in the amount of fluorescence signal depended upon the quantity of IL-1β injected (Fig. 2c). However, the absolute amount of secreted cytokine could not be determined because of the difficulties in controlling the local concentration of cytokines within an open-ended microwell to generate a standard curve. Additionally, immobilized cytokine captured by antibody on the MWA surface was considered to be part of the overall secreted cytokine, while the non-immobilized fraction diffused into the medium. The captured ratio would depend upon an uncontrollable variable, such as the height of the cytokine release point (which determines the probability of the cytokine encountering the capture antibody). Therefore, the assay platform developed in this study was best suited for detection of the onset of secretory molecule secretion from single cells at high time resolution (probably less than 1 min) while also providing semi-quantitative data on secreted molecules. In experiments performed using microwells closed with sealing oil, the platform could detect the signal from 2,000 molecules of IL-1β in a microwell (Supplementary Fig. S5).

Real-time monitoring of IL-6 secretion from single living monocytes within a 1-min time interval. As a proof-of-concept experiment, we assessed the performance of our assay platform for time-resolved observation using lipopolysaccharide (LPS)-stimulated human peripheral blood monocytes by simultaneous detection of cytokine secretion and live/dead signals. We confirmed that proinflammatory cytokines were detected in the culture supernatant of 1×10^5 monocytes stimulated with 1 μg/mL LPS (first priming; Supplementary Fig. S6). Among the detectable cytokines, we selected interleukin 6 (IL-6) as a typical cytokine, known to be released using classical pathways involving ER/Golgi trafficking[11].

First, we examined the reactivity and viability of monocytes in the MWA from snapshot measurements of 2,500 microwells after LPS stimulation for 4 h. Of the 584 cells observed from 2,500 microwells, 23 cells displayed the IL-6 signal (4%). Calcein (+)/SYTOX (−) living cells accounted for 60% of the total cells, but 91% of IL-6–positive cells. Next, 40 microwells were scanned for 4 h for real-time IL-6 secretion imaging at 1-min time intervals. After three independent experiments, we could analyse 71 single cells, including 56 living cells; 7 individual cells were observed to secrete IL-6 (representative images are displayed in Fig. 3a and Supplementary movie 1). IL-6 signals increased gradually for over 1 h after stimulation (Fig. 3b) without change in the SYTOX signal (Fig. 3b), as observed in the displayed dead cell (Fig. 3c). All the remaining IL-6–secreting cells continued to survive during the observation period. These results demonstrated that the single-cell secretion assay platform enabled us to monitor physiological secretion of IL-6 from live monocytes.

Simultaneous imaging of extracellular IL-1β secretion and plasma membrane integrity. The mechanism underlying IL-1β secretion remains poorly understood, although it is known that IL-1β is a key mediator of inflammation[12–14]. Several researchers have proposed various mechanisms for IL-1β secretion[15,16]; however, many details remain to be validated due to a lack of techniques for monitoring real-time secretion processes of IL-1β at single-cell resolution. Therefore, we monitored IL-1β secretion from individual monocytes at high temporal resolution in parallel with observation of the cellular physiological states at the time of secretion.

In this study, monocytes were costimulated with both LPS and adenosine triphosphate (ATP), because IL-1β release from monocytes is known to require a second signal (i.e. ATP) to activate the intracellular inflammasome in addition to priming with pathogen-associated molecular stimuli (i.e. LPS)[17–19]. Glycine was added to the culture medium during stimulation because glycine blocks cytolytic release of pro–IL-1β without affecting the secretion of mature IL-1β (Supplementary Fig. S6)[15,20,21].

Before real-time monitoring, we analysed IL-1β secretion and the live/dead state by snapshot secretion measurements of single cells with calcein/SYTOX staining (Fig. 4a) in 2,500 microwells at 4 h after LPS/ATP stimulation (Supplementary Fig. S7). This snapshot measurement demonstrated that approximately 30% of single monocytes secreted IL-1β. Interestingly, 99% of these IL-1β–secreting cells lost the calcein signal and were stained with SYTOX. When lower LPS concentration (10 ng/mL) was tested, both the number of IL-1β-secreting cells and the amount of secreted IL-1β per monocytes were decreased while the percentage of dead cells was only slightly affected (Supplementary Table S1). The concomitant disappearance of calcein and the increase in SYTOX signal reflect the compromised status of the cell membrane. Therefore, these results suggested some degree of association between IL-1β secretion and the loss of cell membrane integrity, exhibiting a sharp contrast with IL-6 secretion from LPS-stimulated monocytes (in which the vast majority of IL-6 secreting cells remained calcein-positive).

We then performed real-time secretion imaging of IL-1β from monocytes, focusing on whether IL-1β secretion was preceded or followed by a loss of cellular membrane integrity. The experiments

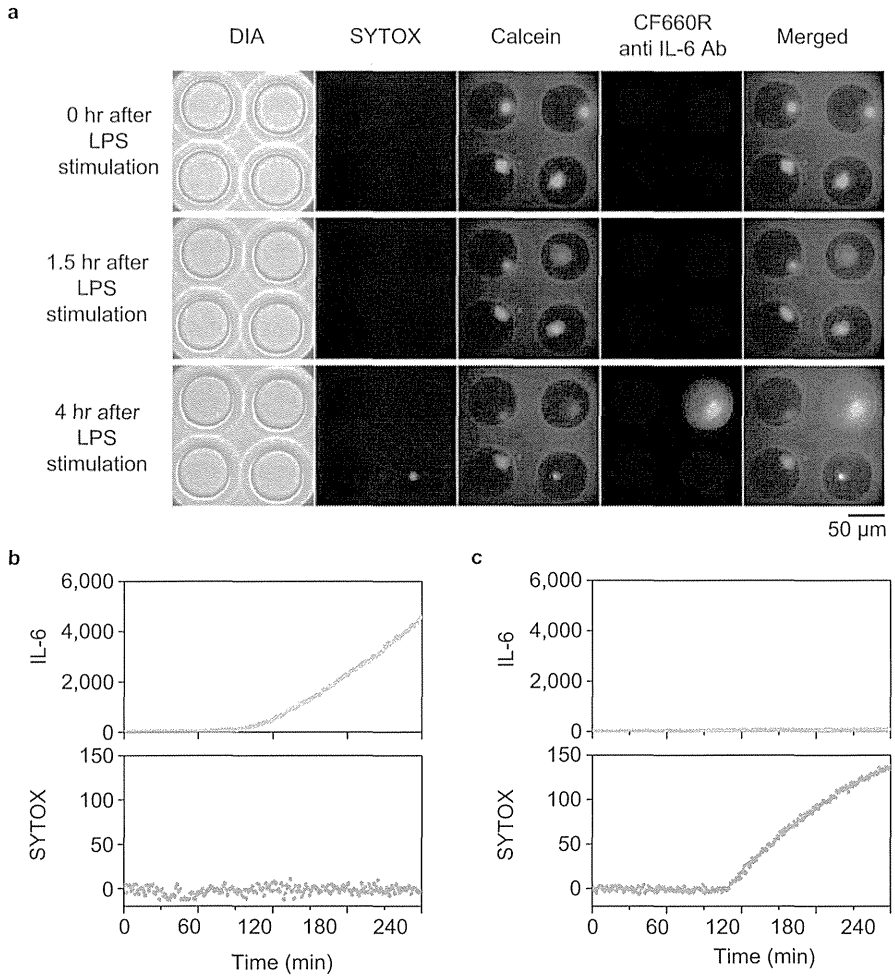

Figure 3 | Time-resolved monitoring of IL-6 secretion after a classical secretion pathway. Calcein-charged human peripheral blood monocytes were introduced into the MWA chip. Signals of SYTOX, calcein and IL-6 secretion were observed with 1-min time intervals after administration of 1 μg/mL of LPS. (a) Representative images of multichannel microscopy. Morphological features of a human monocyte were monitored under diascopic illumination (DIA). The fluorescence signal of SYTOX-stained nuclei was magenta (SYTOX), that of calcein-stained cell bodies was green (Calcein), and that of secreted IL-6 was yellow (CF660R anti IL-6 Ab). Merged images of these three fluorescence signals are also displayed (Merged). Each image was generated at the described time point. Scale bar, 50 μm. Although cells floated soon after LPS stimulation, cells began to adhere to the microwell bottom at 1.5 h after LPS stimulation, with some exhibiting the IL-6 signal at 4 h after LPS stimulation. Although the fluorescence intensity of calcein per pixel was apparently decreased due to the cell deformation, it was distinct from a sharp drop of calcein signal observed for dead cells like in the bottom-right well. The cells that underwent cell death showed elevation of the SYTOX signal. (b), (c) Time course of the average intensity of IL-6 and SYTOX signals within microwells shown in Figure 3a: the top right (b) or the bottom right (c) microwell. (b) The IL-6 secretion signal gradually increased from 80 min after LPS stimulation without any change in SYTOX signal. (c) Typical example of a dead cell. Only the SYTOX signal was increased.

were performed twice, measuring 54 individual monocytes, 20 of which secreted detectable quantities of IL-1β. While all of these cells were calcein-positive before ATP stimulation, they lost their calcein signal and subsequently stained with SYTOX, consistent with the aforementioned snapshot observations (Supplementary movie 2 and Fig. 4b). Disappearance of the calcein signal occurred rapidly and was completed within a few minutes. By contrast, the observed increases in SYTOX signalling consisted of two phases: the first occurred gradually upon ATP stimulation and the second occurred abruptly at various moments following ATP stimulation. These two phases suggest that cell membrane permeability for SYTOX influx was altered through multiple stages.

Surprisingly, IL-1β secretion appeared to coincide with calcein disappearance and the second SYTOX influx (Supplementary movie 2 and Fig. 4c). The increase in the signal of IL-1β secretion occurred as a concave-down function, suggesting IL-1β was secreted in a burst release pattern (Supplementary Fig. S8). To evaluate the association between these events, the transition times were determined by curve fitting of the equation (1), (2), or (3) to the mean fluorescence intensities over time and were compared with one another (Supplementary Fig. S9). Although the response times after ATP stimulation were quite heterogeneous among cells, the transition time of calcein disappearance, SYTOX influx, and IL-1β release were quite similar in most cells (Fig. 5a and b). By focusing on the timeline of these events, lag times between SYTOX influx or IL-1β release and calcein disappearance were calculated. The SYTOX influx and the calcein disappearance (both resulting from membrane imperfections) occurred simultaneously or nearly simultaneously, and SYTOX influx was only slightly delayed following calcein disappearance (mean, 0.2 min; Fig. 5c). By contrast, IL-1β release occurred several minutes following calcein disappearance (mean, 2.0 min, except for 2 outliers; Fig. 5d), and its lag times were more variable than those of SYTOX influx. Two outliers exhibited extremely long delays (44.5 and 105.9 min) in IL-1β release after calcein disappearance. These results indicated that burst release of IL-1β was preceded by loss of cell membrane integrity.

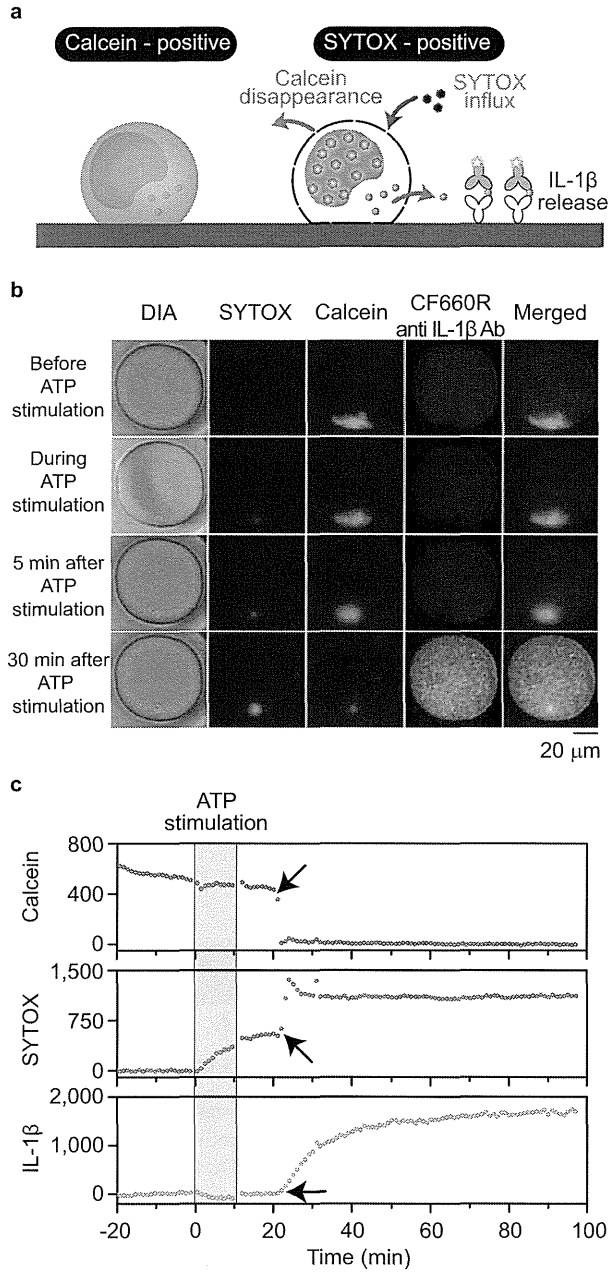

Figure 4 | Time-resolved monitoring of IL-1β secretion on the PDMS MWA chip. (a) Schematic of simultaneous monitoring of IL-1β secretion and cell membrane integrity using calcein and SYTOX staining. SYTOX influx and fluorescent calcein disappearance was observed due to compromised plasma membrane integrity. (b) Representative images of multichannel microscopy. Morphological features of a human monocyte were monitored under diascopic illumination (DIA). The fluorescence signal of SYTOX-stained nuclei was magenta (SYTOX), that of a calcein-stained cell bodies was green (Calcein), and that of secreted IL-1β was yellow (CF660R anti IL-1β Ab). Merged images of these three fluorescence signals are also displayed (Merged). Each image was obtained at the described period. Scale bar, 20 μm. (c) Example of the signal time course during time-resolved monitoring. Grey bands represent the period when the monocytes were exposed to ATP. Arrows represent the transition time of the respective signals.

Discussion

In this study, we have developed a novel assay platform for real-time imaging of secretion at the single cell level at 1-min intervals. The dynamics of cytokine secretion against external stimuli have conventionally been investigated using a bulk population of cells with the same phenotype, based on the premise that these cells always display uniform responses. However, contrary to this premise, we have observed a wide distribution of onset time for IL-1β release triggered by ATP stimulation from individual human peripheral blood monocytes. Temporal heterogeneities at the single cell level have been demonstrated by many studies, but have been limited to intracellular processes, e.g. intracellular calcium elevation[22]. Our results indicated that extracellular reactions, such as protein secretion, were also chronologically heterogeneous at the single cell level. Furthermore, we successfully performed simultaneous measurement of cell membrane integrity and IL-1β release, indicating that our platform allowed for elucidation of the chronological relationship between intracellular process and the extracellular reaction at the single-cell level.

Imaging methods for secretion dynamics have been poorly developed for two primary reasons: First, secreted molecules disperse too rapidly in solution for efficient onsite monitoring. Second, a molecule of interest must be tagged by sensing moieties, but the tagging processes for molecular visualization are often accompanied with greater risks of generating artifacts, including functional modifications. Indeed, this latter point is the most serious limitation of live-cell imaging in general. The platform developed in this study permitted us to bypass such issues by immobilizing and labelling target molecules in the extracellular space. The detection strategy offers an advantage in its non-invasive monitoring of the physiological response of living cells, including clinical samples. A similar methodology with a label-free technique based upon nanoplasmonic imaging has been developed, although it is only applicable to up to three cells per experiment[23]. Sandwich FIA-based assay is expected to be a more sensitive and specific approach for small molecules like cytokines than the plasmonic approach, since the plasmonic signal is proportional to the molecular weight of the binding molecule.

Our platform uses MWAs that effectively trap floating cells as well as secreted cytokine molecules. This compartmentalization permitted integration of independently isolated single cells within a small area to increase the number of observable cells. More specifically, observation of a large number of cells made it feasible to perform statistical analyses on a small population of secreting monocytes. The open architecture of this device is well suited for cell manipulation using conventional tools, allowing for complex experimental arrangements. Additionally, the open architecture was beneficial for the maintenance of cellular physiology, because prolonged isolation within closed microwells may influence cellular conditions, e.g. oxygen starvation[24]. In this work, MWA chips were fabricated with PDMS, suitable for live cell imaging because of its biocompatibility[25]. PDMS offers low cost and fast processing in fabrication of the MWA chip. The only inconvenience was its higher refractive index than that of water, requiring a higher critical angle of the incident light for TIRFM. We resolved the issue by using an objective lens of high numerical aperture to achieve incidence angles greater than the critical angle for a glass/PDMS interface.

In our experiments, the rate of the apparent increase in the TIRF signal was 15 times slower than that of the apparent capture rate of the antigen onto the bottom surface of the MWA chip. This phenomenon was observed probably because (1) the difference in the local concentration of antibodies near the bottom surface and (2) decrease of the unbound antigen by diffusion followed pseudo first-order kinetics with a time constant of approximately 0.9 min (Supplementary Fig. S2). The increase in the concentration of fluorescent detection antibody accelerates the rate of the apparent increase in the TIRF signal while decreasing the detection sensitivity because of elevated background.

The 2,000-molecule detection limit for IL-1β is as low as that reported earlier[6,8]. The average rate of IL-1β secretion from a single monocyte calculated from bulk measurements (Supplementary